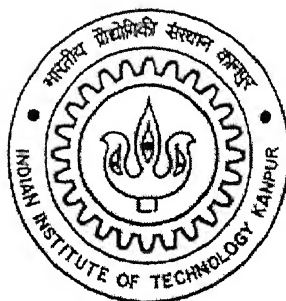


Dielectric Waveguide Tapered optical Coupler

A Thesis Submitted in
Partial Fulfillment of the Requirements
For the Degree of
MASTER OF TECHNOLOGY

by
Sudhanshu Kumar



to the

LASER TECHNOLOGY PROGRAM
INDIAN INSTITUTE OF TECHNOLOGY KANPUR

SEPTEMBER-2004

TH
LT/2004/M
K 96d

TH 2004/LT
मुष्टोत्तम काशीनाथ केलकर पुस्तकालय
भारतीय औद्योगिकी संस्थान कानपुर
एवापि B. A. 152059

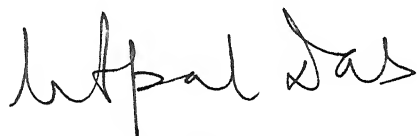


A152059

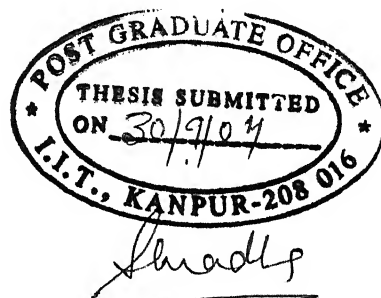
CERTIFICATE

It is certified that the work contained in this thesis titled “**Dielectric Waveguide Tapered optical Coupler**”, by *SUDHANSHU KUMAR* (Y211606), has been carried out under my supervision and this work has not been submitted elsewhere for a degree.

Dr. Utpal Das
Professor and Head LTP
Center for Laser Technology
Indian Institute of Technology Kanpur



September 28, 2004



Acknowledgement

It is my privilege to express my sincere gratitude to Dr. Utpal Das, my thesis supervisor, for his excellent supervision and skilled guidance. I take this opportunity to express my admiration for his brilliance in a gamut of diverse topics. I am also thankful to him for his deep concern towards both my academic and personal life.

I am particularly grateful to my batch-mates Rishi Verma, Rahul Meshram, Promod Kumar Panday, Sukant Kumar Behera and seniors Rajeev Srivastava, R.K Sonkar and S.D Rana for their nice company, which made my stay at IIT Kanpur so enjoyable and cherishable.

I can never adequately thank my mother, my sister and all my family members who encouraged me to study and gave me all support and their LOVE for me all the time. I could reach here only because of my parents.

I.I.T. Kanpur

Sudhanshu Kumar

DEDICATED

TO

MY PARENTS

ABSTRACT

Characteristic matrix method has been used in this work to determine the mode field profile and its evolution in multilayer planar waveguides. The fields in any one layer is expressed as multiplication of the characteristic matrix to the field at its neighboring layer, ultimately relating it to the fields in the substrate layer. Two symmetrical parallel optical waveguide couplers considered that are separated by a center-to-center distance s . The power transfer distance under which the power is completely transferred from wave-guide 1 to wave-guide 2 called coupling length ' L_c ' has been calculated using the normal modes of this multilayer structure. Dependence of ' L_c ' with the thickness of the film (t) rib height (h) rib width (w), waveguide spacing (s) and refractive indices of substrate (n_s) and the film (n_f) have been studied by this technique. Tapered optical waveguide couplers have also been studied by this technique. In the first case the input rib waveguide was tapered (θ) in shape so that width of this waveguide monotonically reduces with distance, whereas the coupled waveguide was kept normal. The separation between the waveguides were kept constant along the length of the coupler. In the second case the input tapered waveguide reduces in width along the length of the coupler, whereas the coupled waveguide increases in width along the length. Single mode planar waveguide structure were thus designed for a rib waveguide use is made of the effective index method to formulate a multilayer planar waveguide and the characteristic matrix method is repeated to obtain the characteristics of the lowest order mode of the rib waveguide. The three cases of coupler i.e. (i) parallel coupler (ii) One waveguide tapered coupler, and (iii) Both waveguides tapered coupler were coupled with respect to its coupling lengths and insertion losses. The coupling lengths were lower for the single tapered case with respect to that of the normal coupler, and for the both waveguide tapered was lower compared to the single waveguide taper. For the both waveguide taper coupler the coupling length decreased with the taper angle (θ) and also with the separation (s). The separation distance was taken to be $s \leq w$. However, separation had little effect on the coupling length where θ was beyond 0.5° . Insertion losses in the three cases are 0.1873 dB, 0.9404 dB and 6.4588 dB respectively.

Contents

Title	i
Certificate	ii
Acknowledgement	iii
Dedication	iv
Abstracts	v
Contents	vi
Chapter 1: Introduction	1
Chapter 2: Multilayer Slab Waveguide	5
2.1 Characteristic Matrix Method	5
2.1.1 TE mode calculation	6
2.1.2 TM mode calculation	9
Chapter 3: Waveguide Analysis	11
3.1 Rib waveguide	11
3.1.1 Effective index method	11
3.2 Quantumwell waveguide	13
3.3 Tapered waveguide	15
Chapter 4: Couplers	17
4.1 Normal mode theory	17
4.1.1 Basic formalism	18
4.2 Tapered coupler	21
4.2.1 Single tapered coupler	21
4.2.2 Double tapered coupler	22
Chapter 5: Results and Discussions	24
Chapter 6: Conclusion	41
References	

Chapter 1

INTRODUCTION

Film waveguides are the basic structure for both the passive and the active devices in integrated optical circuits. The physical principles involved in these waveguides and other related thin-film structures, coupled with those of modern laser electronics, form the foundation of integrated optics. An optical film waveguide is simply a sheet of thin film deposited on a substrate, which has a refractive index, n_f , larger than substrate refractive index n_s , the air-space or cladding refractive index is n_c . Such a three-layered arrangement, with the highest refractive index in the middle layer, forms a lens like medium, which has a natural tendency of focusing a light beam into the film. Because of this focusing action, it is not surprising that a thin film can be used as a waveguide. Consider fig.1.1 where a ray of light starting in the film and propagating toward the upper surface of the film is total internally reflected at the interface of the film and air and the film and substrate. This structure, known as slab waveguide, guides the light beam through the film.

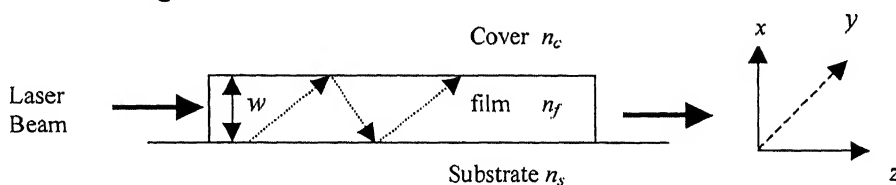


Figure 1.1 Wave propagation in slab waveguide.

Analysis of the field profile of a guided wave is important to understand the coupling of a lightwave from its source to a waveguide and from one waveguide to another waveguide. The mode pattern is the standing wave pattern produced by the interferences in the transverse direction of the optical guide. Some waveguides are designed to have certain mode profile to provide particular spot shape and better coupling efficiency

between different types of waveguides. Moreover, measuring the mode profile is one of the popular methods for characterizing waveguides in practice. Analysis of the mode profiles of a 3-layer slab waveguide, which provides, such guide characteristics as the effective guide index and effective guide width, is dependent on waveguide parameters. These are the refractive indices n_s , n_f and n_c of the substrate, the film and the cover respectively. The film thickness w and the free space wavelength λ or propagation constant, $k_0=2\pi/\lambda = \omega/c$ of the light. The number of independent parameters can be combined by the introduction of appropriate normalized parameters to provide universal plots from which the effective index and effective guided thickness can be determined for any slab waveguide configuration, this will be discussed in chapter 2. For basic guide parameter the normalized frequency or normalized film thickness V , defined as:

$$V = k_0 w \sqrt{n_f^2 - n_s^2}$$

The mode profile of a 3-layer slab waveguide can be carried out in a straightforward manner [1], special methods have been developed for more complex structures. Well known among these are the characteristic matrix method [2], finite element method, Fourier expansion method, and discrete sine method.

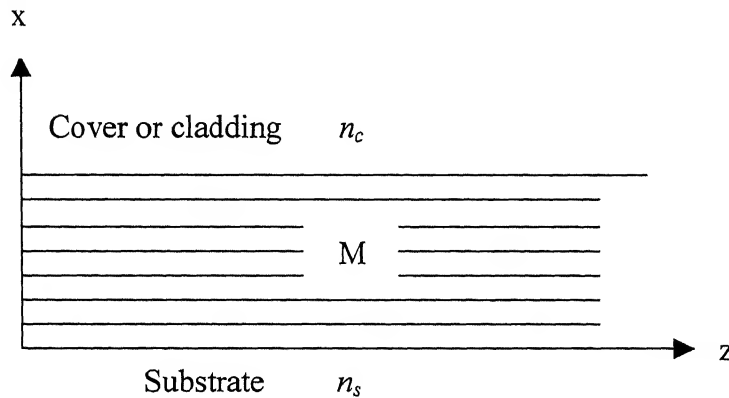


Figure 1.2 Sketch of a multilayer slab waveguide with substrate index n_s and cover index n_c . The y-axis indicates the direction of mode propagation.

The characteristic matrix method has been used to analyze the coupling in thin film as well as the analysis of multilayer planar waveguides. Here the characteristic matrix method is used for its application to study the mode profile as well as its evolution in y -invariant planar waveguides with arbitrary refractive index profile. This method will be shown to be relatively simple and requires only modest computational power. Guided mode fields extend outside the guiding region into the surrounding cladding medium, called evanescent field, decaying exponentially away from the waveguide cladding boundary. For two waveguides close together such that the evanescent fields of the propagating modes in two waveguides overlap, there exists coupling of optical power between the two waveguides. Such a device is called a directional coupler. The fraction of power coupled per unit length from one waveguide to the other is determined by the overlap of the modes between the two waveguides as shown in fig. 1.3.

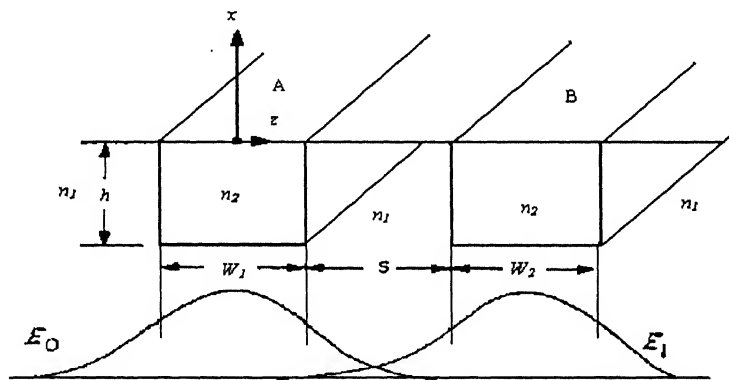


Figure 1.3 Electric field profile in symmetrical coupler.

Thus it depends on the separation of the guides, the mode penetration into the substrate, and the interaction length. This energy exchange can be used in building an optical modulator or optical switch. Fig. 1.4 shows a directional coupler consisting of two single mode waveguides, which are in close proximity over a length L_c . When the incident light is focused into a single channel at $y=0$, then there is a periodic exchange of energy between the two waveguides. If the propagation constants of the modes in the

waveguides are identical then there is a complete transfer of energy from one waveguide to the other over a length " L_c " and if the propagation constant is not identical then there is only an incomplete transfer of energy for the same length i.e. the coupling length L_c become different.

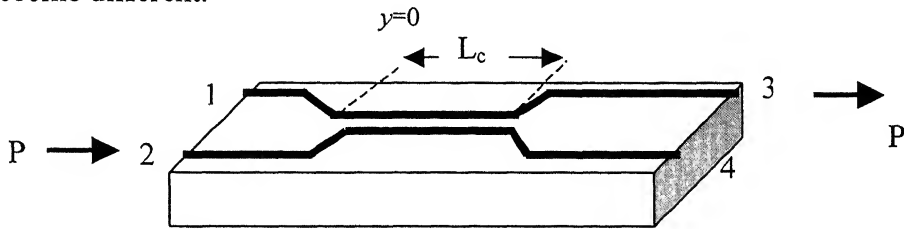


Figure 1.4 Optical directional coupler in which two waveguides are at close proximity over a length L_c .

A theoretical analysis of the coupling between two dielectric waveguide usually involves a formal solution of Maxwell's equation using matrix method, when the waveguide modes have significant overlap. The waveguides can have any arbitrary cross-section however for the sake of simplicity only guides with rectangular cross-sections have been considered here. In the following chapters, chapter 2 discuss the matrix method used to establish the mode field profiles and propagation constants of multilayered slab waveguides. Chapter 3 discusses the analysis of multilayer rib waveguides using the effective index method. Hence the quasistatic modal field and propagation constant for a tapered waveguide along its length have also been discussed. Coupled mode analysis have been carried out in chapter 4 for parallel waveguide couplers, however a matrix method is developed for asymmetric as well as tapered waveguide coupler using the lowest order mode in the effective index method. The result of all the analysis is presented in chapter 5. Hence the field profiles as well as power profiles of tapered waveguide couplers are presented. From this the coupling lengths of tapered couplers are obtained and compared with parallel waveguide couplers. Chapter 6 concludes this work.

Chapter 2

Multilayer Slab Waveguide

2.1 Characteristic Matrix Method

A z-invariant multilayer planar waveguide with $p+2$ layers is shown in fig. 2.1. This structure can represent either step index waveguides or a stepwise approximation to graded index waveguides. The waveguide medium is assumed to be linear, lossless, source free and non-magnetic. Light is propagated along positive z direction. In order to simplify the analysis, TE and TM polarization field will be considered separately, in rectangular coordinates system field vector F (E or H) expressed as

$$F = F(x, y)e^{-j\beta z} \quad (2.1)$$

where β is called propagation constant of guide

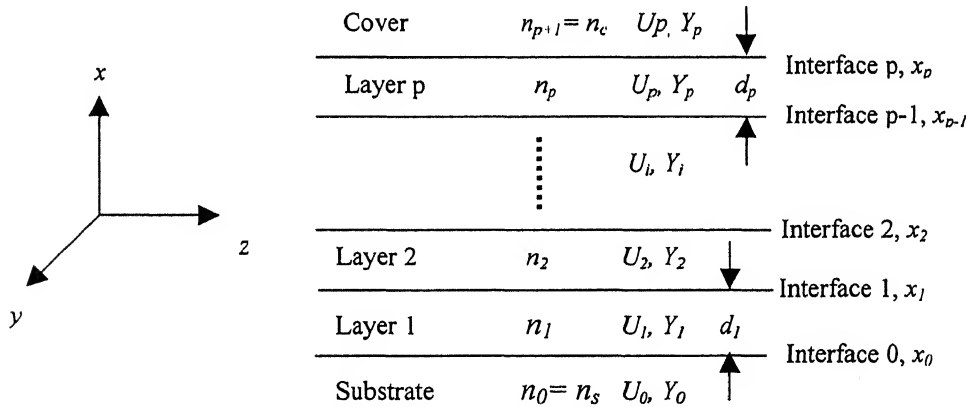


Figure 2.1 Multilayer planer waveguide structure

2.1.1 Transverse and Axial fields

The first two Maxwell's equations are represented as

$$\nabla \times H = (\sigma + j\omega\epsilon)E \quad (2.2)$$

$$\nabla \times E = -j\omega\mu H \quad (2.3)$$

where σ and ϵ represents the conductivity and permittivity of the dielectric respectively.

For a rectangular coordinate system with $\sigma=0$, Maxwell's Eq. (2.2) and Eq. (2.3) yield the scalar equations

$$-j\omega\mu H_x = j\beta E_y + \frac{\partial E_z}{\partial y} \quad (2.4)$$

$$-j\omega\mu H_y = -j\beta E_x - \frac{\partial E_z}{\partial x} \quad (2.5)$$

$$-j\omega\mu H_z = \frac{\partial E_y}{\partial x} - \frac{\partial E_x}{\partial y} \quad (2.6)$$

$$j\omega\varepsilon E_x = j\beta H_y + \frac{\partial H_z}{\partial y} \quad (2.7)$$

$$j\omega\varepsilon E_y = -j\beta H_x - \frac{\partial H_z}{\partial x} \quad (2.8)$$

$$j\omega\varepsilon E_z = \frac{\partial H_y}{\partial x} - \frac{\partial H_x}{\partial y} \quad (2.9)$$

2.1.2 TE Polarization Mode

For TE polarization, $E_x=0$, $E_z=0$ and $H_y=0$, the Maxwell's equations lead to the relations

$$H_x = -\frac{\beta}{\omega\mu} E_y \quad (2.10)$$

$$\frac{\partial E_y}{\partial x} = -j\omega H_z \quad (2.11)$$

$$\frac{\partial H_z}{\partial x} + j\beta H_x = -j\varepsilon_0 n^2 \omega E_y \quad (2.12)$$

By defining new variables $U = E_y$ and $Y = \omega\mu H_z$, the equations are converted to

$$U' = -jY \quad (2.13)$$

$$U'' + k^2 U = 0 \quad (2.14)$$

where $U' = \partial U / \partial x$; $U'' = \partial^2 U / \partial x^2$; $k^2 = k_0^2 n^2 - \beta^2$; $k_0 = 2\pi / \lambda$

and n is the refractive index of the layer under consideration

Solutions of Eq. (2.13) and Eq. (2.14) in the layer have the general forms

$$U(x) = A \exp(-jkx) + B \exp(jkx) \quad (2.15)$$

$$Y(x) = k[A \exp(-jkx) - B \exp(jkx)] \quad (2.16)$$

By applying boundary conditions, U and Y at any interface plane can be related with its adjacent planes by means of the characteristic matrix associated with the layer in between expressed by

$$\begin{bmatrix} U_i \\ Y_i \end{bmatrix} = M_i \begin{bmatrix} U_{i-1} \\ Y_{i-1} \end{bmatrix} \quad (2.17)$$

where the characteristic matrix M_i is given as

$$M_i = \begin{bmatrix} \cos(k_i d_i) & -j \sin(k_i d_i) / k_i \\ -j k_i \sin(k_i d_i) & \cos(k_i d_i) \end{bmatrix} \quad (2.18)$$

Eq. (2.17) is generalized to give the relation

$$\begin{bmatrix} U_i \\ Y_i \end{bmatrix} = M_T \begin{bmatrix} U_0 \\ Y_0 \end{bmatrix} \quad (2.19)$$

$$\text{where } M_T = M_i M_{i-1} \dots \dots \dots M_2 M_1 = \begin{bmatrix} m_{i11} & m_{i12} \\ m_{i21} & m_{i22} \end{bmatrix} \quad (2.20)$$

If decay constant in substrate is γ_s then, Eq. (2.15) and Eq. (2.16) can be written as

$$U_s(x) = U_0 \exp(\gamma_s x) \quad (2.21)$$

$$Y_s(x) = j\gamma_s U_s \quad (2.22)$$

where $\gamma_s^2 = \beta^2 - n_s^2 k_0^2$ at interface 0, we obtain

$$U_0 = U_s(0) \quad (2.23)$$

$$Y_0 = Y_s(0) = j\gamma_s U_0 \quad (2.24)$$

In terms of U_0 and Y_0 , the values of U and Y at any point x , between x_i and x_{i+1} can be obtained by envisioning a virtual interface at x , according to

$$\begin{bmatrix} U(x) \\ Y(x) \end{bmatrix}_{x_i \leq x \leq x_{i+1}} = \begin{bmatrix} \cos(k_{i+1}(x - x_i)) & -j \sin(k_{i+1}(x - x_i)) / k_{i+1} \\ -jk_{i+1} \sin(k_{i+1}(x - x_i)) & \cos(k_{i+1}(x - x_i)) \end{bmatrix} \times \begin{bmatrix} U_0 \\ Y_0 \end{bmatrix} \quad (2.25)$$

$$\text{which result in} \quad U(x)_{x_i \leq x \leq x_{i+1}} = f(x)_{x_i \leq x \leq x_{i+1}} U_0 \quad (2.26)$$

where

$$f(x)_{x_i \leq x \leq x_{i+1}} = (m_{i11} + j\gamma_s m_{i12}) \cos(k_{i+1}(x - x_i)) - \frac{j(m_{i21} + j\gamma_s m_{i22}) \sin(k_{i+1}(x - x_i))}{k_{i+1}} \quad (2.27)$$

If decay constant in cover or cladding is γ_c then the value of U and Y in the cover can be similarly obtained by writing

$$U_c(x) = B_c \exp(-\gamma_c x) \quad (2.28)$$

$$Y_c(x) = -j\gamma_c U_c \quad (2.29)$$

where $\gamma_c^2 = \beta^2 - n_c^2 k_0^2$ at the interface p , we have

$$\begin{bmatrix} U_p \\ Y_p \end{bmatrix} = \begin{bmatrix} B_c \exp(-\gamma_c x_p) \\ -j\gamma_c B_c \exp(-\gamma_c x_p) \end{bmatrix} = M_p \begin{bmatrix} U_0 \\ Y_0 \end{bmatrix} \quad (2.30)$$

which result in

$$U_c(x) = g \exp(-\gamma_c x) U_0 \quad (2.31)$$

where

$$g = \frac{j\gamma_c m_{p11} - \gamma_c \gamma_s m_{p12} - m_{p21} - jm_{p22} \gamma_s}{2j\gamma_c \exp(-\gamma_c x_p)} \quad (2.32)$$

From Eq. (2.30), we obtain the dispersion relation for TE modes

$$j(\gamma_s m_{p22} + \gamma_c m_{p11}) = \gamma_s \gamma_c m_{p12} - m_{p21} \quad (2.33)$$

For TE modes parameter “ b ” is called the normalized guide index [1] and which is defined by

$$b = \frac{(n_{eff}^2 - n_s^2)}{(n_f^2 - n_s^2)} \quad (2.34)$$

where n_{eff} is the effective index of waveguide, defined as β/k_0 .

2.1.3 TM Polarization Mode

For TM-polarized mode, $H_x=0$, $H_z=0$ and $E_y=0$, the following notation is introduced

$$U = H_y \quad (2.35)$$

$$Y = \omega \varepsilon_0 E_z \quad (2.36)$$

This leads to a solution of the wave equation as

$$U(x) = A \exp(-jkx) + B \exp(jkx) \quad (2.37)$$

$$Y(x) = -\frac{k}{n^2} [A \exp(-jkx) - B \exp(jkx)] \quad (2.38)$$

The characteristic matrix is then given by

$$M_i = \begin{bmatrix} \cos(k_i d_i) & -jn_i^2 \sin(k_i d_i) / k_i \\ -jk_i \sin(k_i d_i) / n_i^2 & \cos(k_i d_i) \end{bmatrix} \quad (2.39)$$

For the mode fields in substrate again

$$U_s(x) = U_0 \exp(\gamma_s x) \quad (2.40)$$

$$Y_s(x) = -\frac{j}{n_s^2} \gamma_s U_s = -\frac{j}{n_s^2} \gamma_s U_0 \exp(\gamma_s x) \quad (2.41)$$

Following the same formulation described for the TE case, one may write for TM

$$U(x)_{x_i \leq x \leq x_{i+1}} = f(x)_{x_i \leq x \leq x_{i+1}} U_0 \quad (2.42)$$

with

$$f(x)_{x_i \leq x \leq x_{i+1}} = (m_{i11} - j \frac{\gamma_s}{n_s^2} m_{i12}) \cos(k_{i+1}(x - x_i)) + \frac{n_{i+1}^2}{k_{i+1}} (j m_{i21} + \frac{\gamma_s}{n_s^2} m_{i22}) \sin(k_{i+1}(x - x_i)) \quad (2.43)$$

Similarly for the field in cover layer, we have

$$U_c(x) = g \exp(-\gamma_c x) U_0 \quad (2.44)$$

with

$$g = \left(m_{p_{11}} - j \frac{\gamma_s}{n_s^2} m_{p_{12}} \right) \exp(\gamma_c x_p) \quad (2.45)$$

and corresponding dispersion relation is given as

$$-j \left(\frac{m_{p_{22}} \gamma_s}{n_s^2} + \frac{m_{p_{11}} \gamma_c}{n_c^2} \right) = \frac{\gamma_s \gamma_c m_{p_{12}}}{n_s^2 n_c^2} - m_{p_{21}} \quad (2.46)$$

For TM modes the normalized guided index b [1] is defined by

$$b = \frac{(n_{eff}^2 - n_s^2)}{(n_f^2 - n_s^2)} \left(\frac{n_f^2}{n_s^2 q_s} \right) \quad (2.47)$$

where n_{eff} is the effective index of waveguide and the reduction factor q_s is given by:

$$q_s = \frac{n_s^2 / n_f^2}{(1 - b) + b n_s^4 / n_f^4} \quad (2.48)$$

For a waveguide with known geometric structures, excited at a known wavelength, the propagation constant β and the number of guided modes for TE and TM polarization may be obtained by solving Eq. (2.33) and Eq. (2.46) respectively. Hence, the electric field profile $E_y(x)$ in substrate, cladding and central layer for TE polarization mode can be obtained from Eq. (2.21), Eq. (2.31) and Eq. (2.26) respectively while the magnetic field profile $H_y(x)$ in substrate, cladding and central layer for the TM-polarization mode can be obtained from Eq. (2.40), Eq. (2.44), and Eq. (2.42) respectively.

Chapter 3

Waveguide Analysis

3.1 Rib Waveguide

For a N-layer rib waveguide, the refractive index values n_s (substrate), n_1, \dots, n_N (Layers 1 to N), n_c (cover), the thicknesses t_1, \dots, t_N of the inner layers, the etching depth h , and the width w of the rib. All dimensions are meant in micrometers. The figure illustrates the relevant geometry

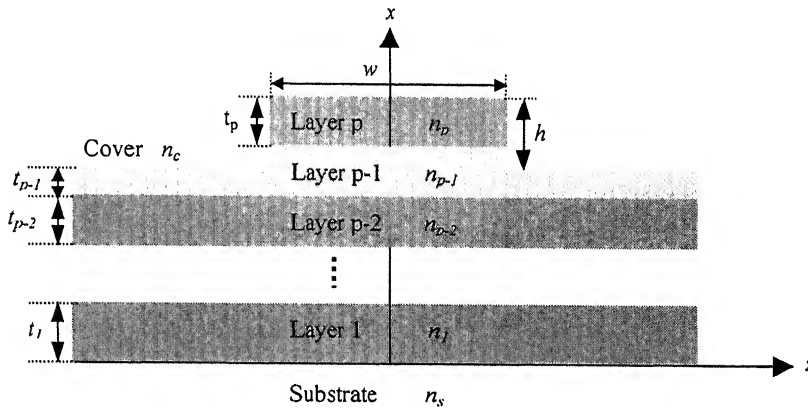


Figure 3.1 Multilayer rib waveguide structure

Note the orientation of the transverse coordinate axes with the x -direction perpendicular to the film plane. Light propagates along the z -direction. The entire structure is meant to be symmetric with respect to the x - z plane. The structure informs about propagation constants β (μm^{-1}) and effective mode indices n_{eff} . The effective index simulation starts with computing the one-dimensional modes of the central slice $-w/2 < z < w/2$ and the two identical lateral slices $z < -w/2$ and $w/2 < z$.

3.1.1 Effective Index Method

In this method, the effective index (EI) of the structure is obtained by successively solving two transcendental slab equations. If the example of a rib waveguide is considered, fig.3.2 (a), then the method in the first step solves the transcendental equations for three vertical

slabs as shown in fig.3.2 (b). The effective indices n_{eff1} and n_{eff2} so obtained are used as the refractive indices for a 3-layer horizontal slab waveguide, as shown in fig.3.2(c). Solving the transcendental equation for the horizontal slab waveguide gives a good approximation to the effective index of the original rib waveguide structure, for the lowest order mode. The advantage of the EI method is that it can be applied to a wide variety of structures.

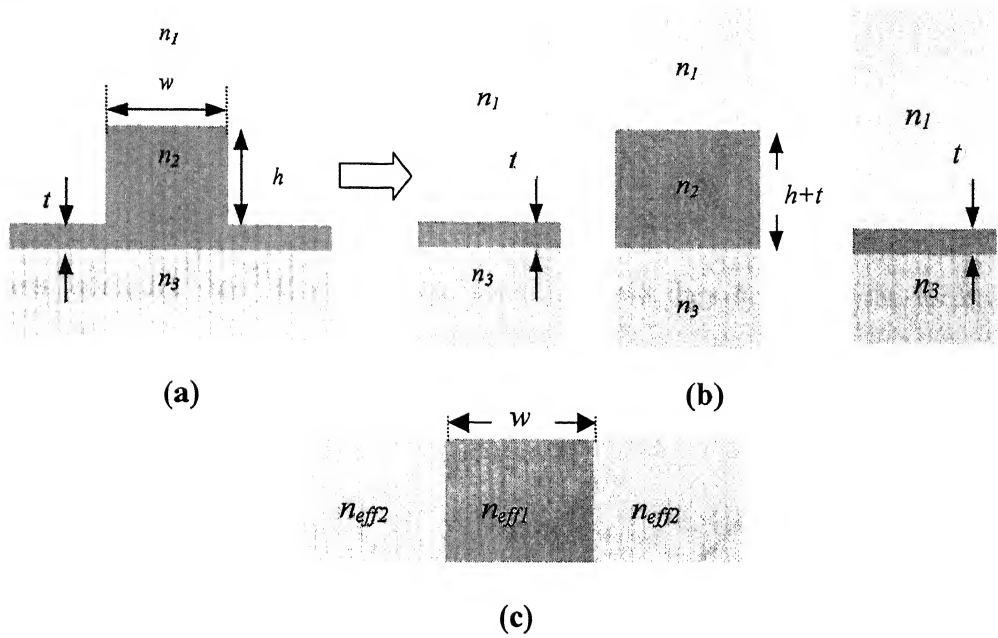


Figure 3.2 The Effective Index method for the rib waveguide (a) the original rib waveguide, (b) solving the vertical slab problem to define n_{eff1} and n_{eff2} (step 1), (c) equivalent horizontal slab structure (step2)

For TE modes the normalized guided indices b is defined by

$$b = \frac{(n_{eff}^2 - n_{eff2}^2)}{(n_{eff1}^2 - n_{eff2}^2)} \quad (3.1)$$

where n_{eff1} , n_{eff2} and n_{eff} are the effective index of inner, outer regions and overall structure respectively.

The normalized frequency or film thickness V for final structure will be

$$V = k_0 w (n_{eff1}^2 - n_{eff2}^2)^{1/2} \quad (3.2)$$

where w is the width of central region and $k_0 = 2\pi/\lambda$.

The mode profile plots show the field of the basic electric component E_y for TE-like modes and of the basic magnetic component H_y for TM-like modes. Note that the effective index approximation assumes factorizing mode fields one due to lateral and another are due to central slice. Hence the horizontal profile yields the correct y -dependence for all positions x . According to the initial decomposition in vertical slices, there are two different vertical profiles, one corresponding to the central region and one for the lateral slices. These curves are the constituting 1-D mode profiles.

3.2 Quantum Well Waveguide

When dimension of the semiconductor becomes comparable to the mean free path (mfp) of carriers, quantum size effects become important and they dominate the electronic properties of the material. Of particular interest are quantum well structures [3], show in fig.3.3.

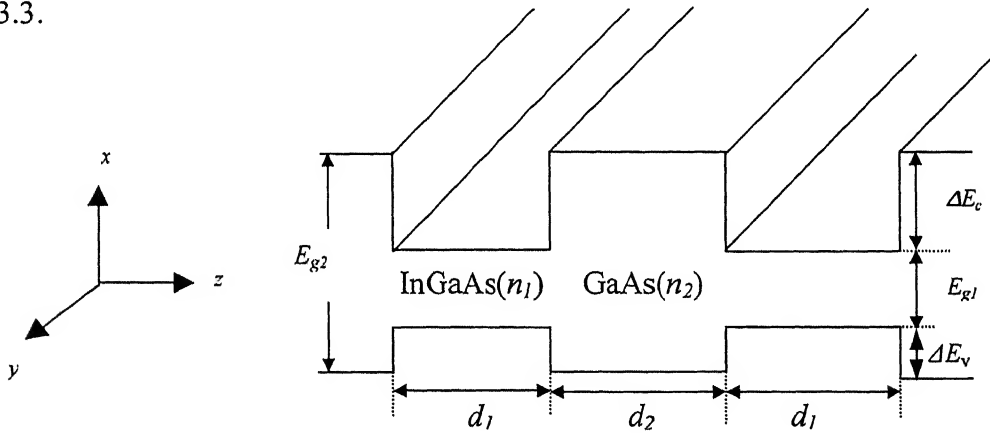


Figure 3.3 Schematic representation of a quantum well in three dimensions formed by two semiconductors with bands E_{g1} (InGaAs) and E_{g2} (GaAs). d_1 and d_2 are well and barrier widths respectively.

In such structures two semiconductors of different band gap energies alternate to form a synthetically modulated structure. If the narrow gap semiconductor layer thickness is comparable to the mfp of electrons in the material, the motion of carriers in the direction perpendicular to the interfaces is quantized. If the thicknesses of the wide-bandgap layers are thin enough, such that carriers may tunnel through, the discrete

energy levels formed in the quantum wells due to size quantization splits into minibands. Such a composite material is called a superlattice, which has electronic and optical properties that are unique to the whole structure. For example, carriers are transported through such material by miniband conduction. Also, the effective bandgap of entire composite structure is approximately equal to the energy separation between electron and hole minibands.

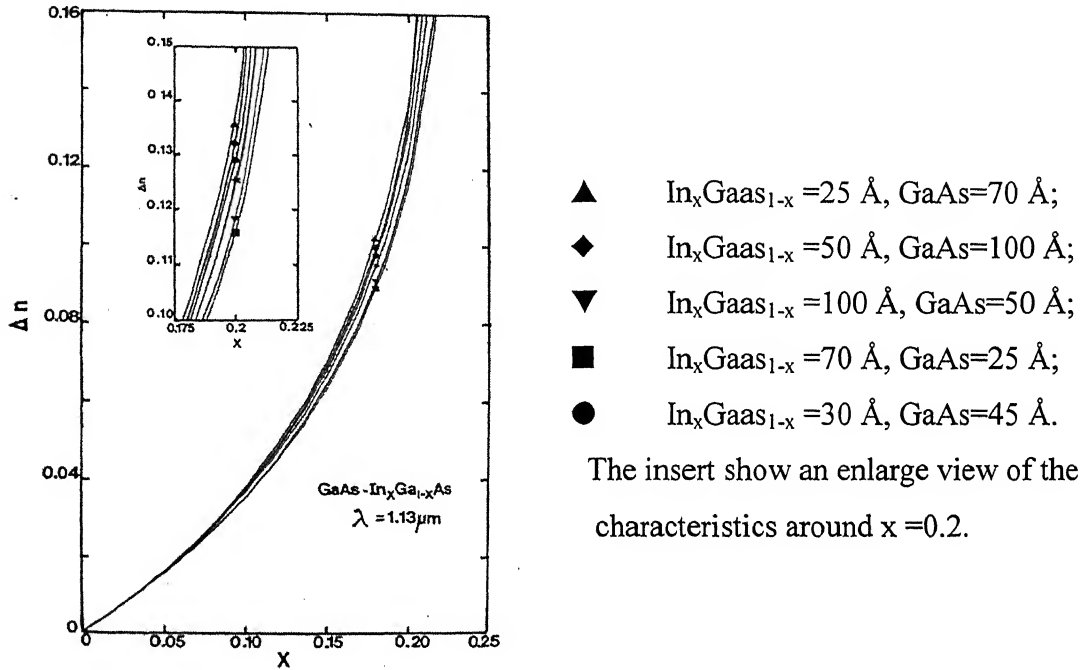


Figure 3.4 Refractive index step between $\text{In}_x\text{Ga}_{1-x}\text{As}$ and GaAs for different values of x as indicated by the representative symbol [4]

Usually in compound semiconductor materials with $E_g \cong 1\text{eV}$, such coupling between wells occurs for barrier thickness $\leq 5\text{nm}$. For barrier thickness larger than 5nm , the individual well are largely uncoupled and the electronic properties in a single-quantum well (SQW) or multiquantum well (MQW) are quite similar. In general the refractive index of a strained $\text{In}_x\text{Ga}_{1-x}\text{As}$ is given as [4]

$$n_1 = n_2 + \Delta n \quad (3.4)$$

where Δn is shown in fig.3.4.

So the refractive index a MQW of GaAs/In_xGa_{1-x}As is

$$\bar{n}_f = \frac{n_1 d_1 + n_2 d_2}{d_1 + d_2} \quad (3.3)$$

The value of \bar{n}_f for a specific structure as shown in fig.3.5 can be calculated using the Δn [4].

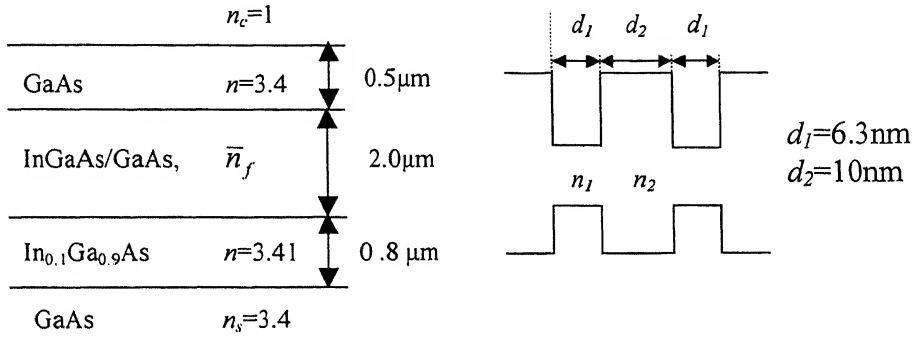


Figure 3.5 Schematic representations of n⁺GaAs quantum well structure.

3.3 Tapered Waveguide

In the given structure of a tapered waveguide fig.3.6, if signal is incident at the end B (w_2) it will propagate through the structure and finally it reaches at the end A (w_1) but

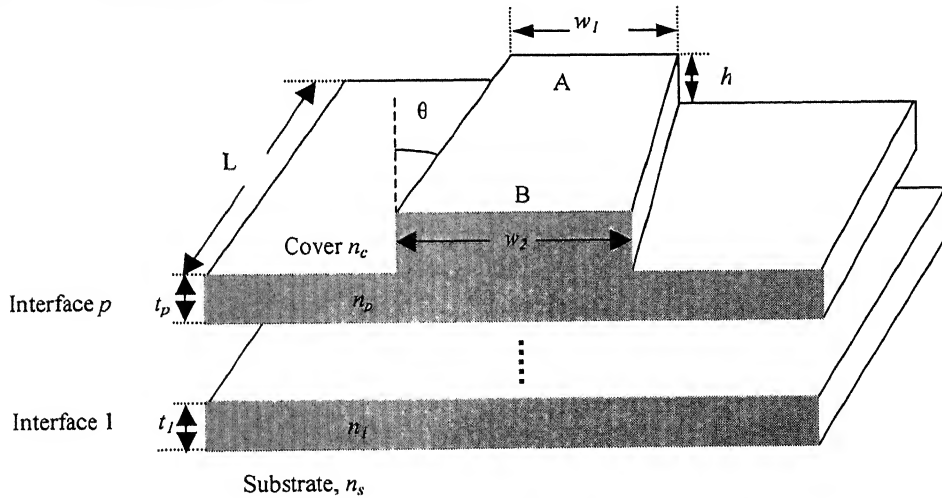


Figure 3.6 Schematic representation of multilayer tapered waveguide.

due to tapered structure of the rib its modal width changes and so does the propagation constant. The effective index method be used in the equivalent waveguide

structure as shown in fig.3.7, where at different y the modal profile and the propagation constant will be different, under the quasistatic approximation.

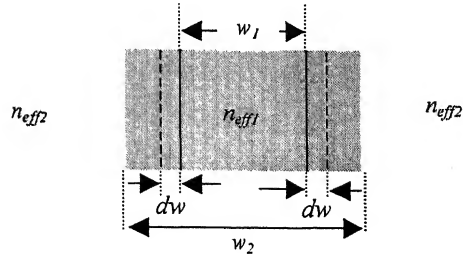


Figure 3.7 The equivalent waveguide representation of multilayer tapered waveguide,

n_{eff2} and n_{eff1} are effective indices of lateral and central slice of the structure.

Chapter 4

Couplers

4.1 Normal Mode Analysis

Instead of coupled waveguide analysis, another approach of great practical interest is coupling of the normal in the steady state of the composite structure. For example, two parallel optical waveguides are coupled to each other via their evanescent fields. A wave set up initially in one guide is transferred to the other guide. Another coupling is affected between forward and backward waves by periodic perturbations on an optical waveguide. This process is also akin to the coupling of the normal mode analysis [5] presented here.

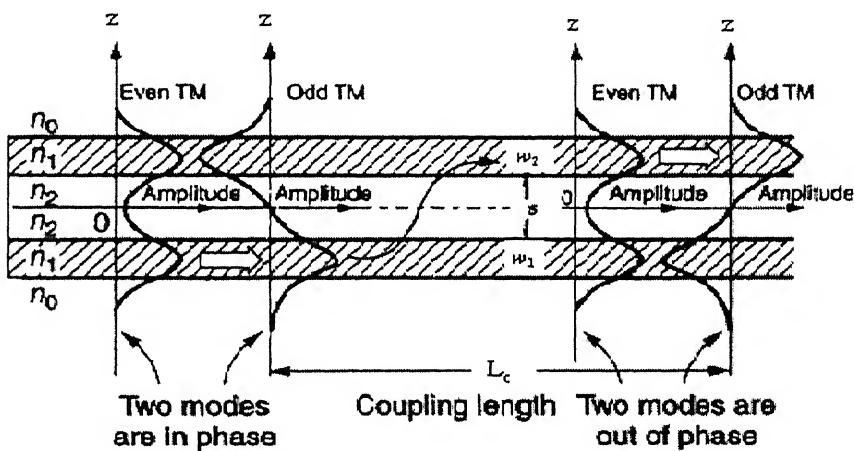


Figure 4.1 Slab optical coupler with symmetry in the refractive index distribution.

Fig.4.1 [6], correspond to the two lowest order modes of the pair of waveguides in a directional coupler considered as a single waveguide structure. Energy incident on one waveguide can be considered to be a linear combination of the two modes, which is shown in the above figure. As the modes propagate in the waveguides, they develop a phase difference due to difference in β values of the two modes. Thus at some point a

phase difference of π is developed which corresponds to the total energy in the other waveguide.

4.1.1 Basic formalism

Consider two waves $a_1(y)$ and $a_2(y)$, of modes 1 and 2, which in the absence of coupling have propagation constants β_1 and β_2 . They obey the equations

$$\frac{da_1}{dy} = -i\beta_1 a_1(y) \quad (4.1)$$

$$\frac{da_2}{dy} = -i\beta_2 a_2(y) \quad (4.2)$$

Suppose next that the two waves are weakly coupled by some means, so that $a_1(y)$ is affected by $a_2(y)$ and $a_2(y)$ is affected by $a_1(y)$. Then, the equations become

$$\frac{da_1}{dy} = -i\beta_1 a_1(y) + \kappa_{12} a_2(y) \quad (4.3)$$

$$\frac{da_2}{dy} = -i\beta_2 a_2(y) + \kappa_{21} a_1(y) \quad (4.4)$$

where the constants κ_{12} and κ_{21} represents the strength of interaction between the two modes and referred to as coupling constants, in the absence of any interaction between the two modes $\kappa_{12} = \kappa_{21} = 0$. The above equations show that in the presence of interaction, the amplitude of the mode in a waveguide depends on the amplitude of the mode in the other waveguide. The coupling constants depend upon the waveguide parameters, the separation between the waveguides and the wavelength of operation. For identical waveguides one can show that

$$\kappa_{21} = \kappa_{12} \quad (4.5)$$

In order to solve this set of equations, the solution will be

$$a_1(y) = a_1(0) \exp(-i\beta_1 y) \quad (4.6)$$

$$a_2(y) = a_2(0) \exp(-i\beta_2 y) \quad (4.7)$$

the existence of a wave in the system consisting of the two coupled waveguide, which propagates with a phase constant β and which is a superposition of the modes of waveguides 1 and 2 with amplitude $a_1(0)$ and $a_2(0)$. Substituting from Eq. (4.6) and (4.7) in Eq. (4.3) and (4.4)

$$-i\beta a_1(0) = -i\beta_1 a_1(0) - i\kappa_{12} a_2(0) \quad \text{at } y=0$$

$$a_1(0)(\beta - \beta_1) - \kappa_{12} a_2(0) = 0 \quad (4.8)$$

$$a_2(0)(\beta - \beta_2) - \kappa_{21} a_1(0) = 0 \quad (4.9)$$

solve the above two equations Eq. (4.8) and Eq. (4.9)

$$\beta^2 - \beta(\beta_1 + \beta_2) + (\beta_1 \beta_2 - \kappa^2) = 0 \quad (4.10)$$

where $\kappa = (\kappa_{12} \kappa_{21})^{1/2}$; thus

$$\beta_{s,a} = \frac{1}{2}(\beta_1 + \beta_2) \pm \left[\frac{1}{4}(\beta_1 - \beta_2)^2 + \kappa^2 \right]^{1/2} \quad (4.11)$$

Thus, in the coupled waveguide, one has two independent sets of modes, one propagating with propagation constant β_s and the other with β_a . Therefore the general solution of Eq. (4.3) and Eq. (4.4) can be written as

$$a_1(y) = a_s \exp(-i\beta_s y) + a_a \exp(-i\beta_a y) \quad (4.12)$$

$$a_2(y) = \frac{\beta_s - \beta_1}{\kappa_{12}} a_s \exp(-i\beta_s y) + \frac{\beta_a - \beta_1}{\kappa_{12}} a_a \exp(-i\beta_a y) \quad (4.13)$$

It is noted that when the two waveguides are identical then $\beta_1 = \beta_2 = \beta_0$

$$\beta_s = \beta_0 + \kappa \quad (4.14)$$

$$\beta_a = \beta_0 - \kappa \quad (4.15)$$

and we have for the mode with propagation constant $\beta = \beta_s$

$$a_1(0) = a_2(0) \quad (4.16)$$

and for the mode with propagation constant $\beta = \beta_a$

$$a_1(0) = -a_2(0) \quad (4.17)$$

We now assume that at $y=0$, the mode in waveguide 1 is launched with unit power and that there is no power in waveguide 2. Then we have the $y=0$ initial conditions,

$$a_s + a_a = 1 \quad (4.18)$$

$$\frac{\beta_s - \beta_1}{\kappa_{12}} a_s + \frac{\beta_a - \beta_1}{\kappa_{12}} a_a = 0 \quad (4.19)$$

which gives $a_s = \frac{\beta_1 - \beta_a}{\beta_s - \beta_a}$; and $a_a = -\frac{\beta_1 - \beta_s}{\beta_s - \beta_a}$

The power in waveguide 1 and 2 is proportional to $|a_1(y)|^2$ and $|a_2(y)|^2$ respectively.

$$|a_1(y)|^2 = 1 - \frac{\kappa^2}{(\Delta\beta/2)^2 + \kappa^2} \sin^2 \left[((\Delta\beta/2)^2 + \kappa^2)^{1/2} y \right] \quad (4.20)$$

$$|a_2(y)|^2 = \frac{\kappa^2}{(\Delta\beta/2)^2 + \kappa^2} \sin^2 \left[((\Delta\beta/2)^2 + \kappa^2)^{1/2} y \right] \quad (4.21)$$

where $\Delta\beta = \beta_1 - \beta_2$

As can be seen from Eq. (4.20) and Eq. (4.21), there is a periodic exchange of energy between the two waveguides with a period

$$l = \frac{\pi}{((\Delta\beta/2)^2 + \kappa^2)^{1/2}} \quad (4.22)$$

Hence the length

$$L = l/2 = \frac{\pi}{2((\Delta\beta/2)^2 + \kappa^2)^{1/2}} \quad (4.23)$$

This is the minimum interaction length under which max power can transfer it is called coupling length of the directional coupler. From Eq. (4.23), it is clear that complete power transfer can take place when $\Delta\beta=0$, i.e. the propagation constants of the mode in each waveguide are same. Then coupling length will be

$$L_c = \frac{\pi}{2\kappa} = \frac{\pi}{(\beta_s - \beta_a)} \quad (4.24)$$

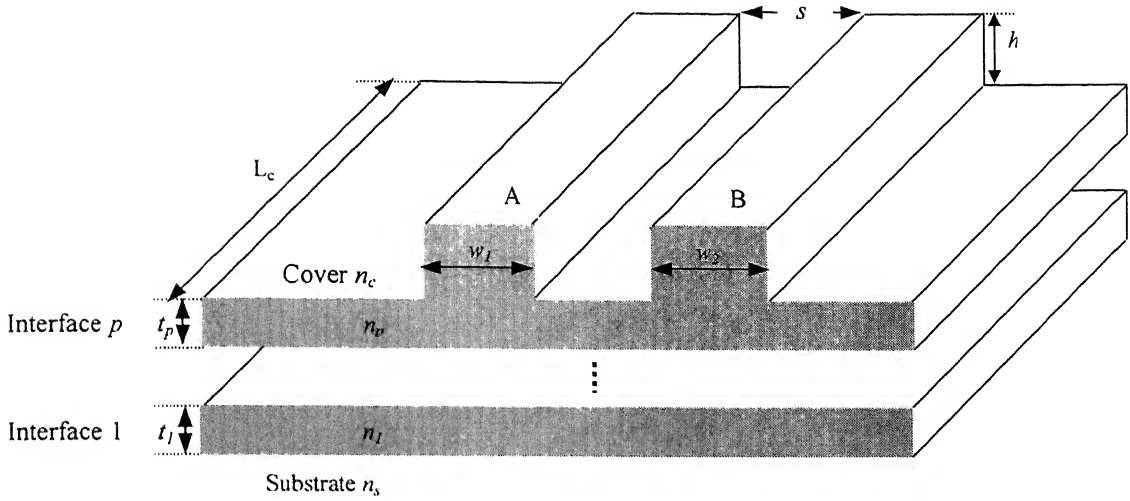


Figure 4.2 Schematic representation of multilayer symmetric coupler.

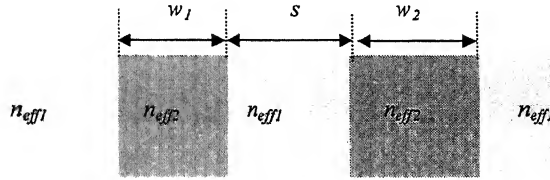


Figure 4.3 The equivalent waveguide representation of multilayer symmetrical coupler.

4.2 Tapered Coupler

4.2.1 Single Tapered Coupler

A typical corrugated single tapered waveguide coupler is shown in fig 4.4. This structure has two rib waveguides A and B separated by distance s , A is tapered rib waveguide of tapering angle θ and waveguide B a parallel rib waveguide, the etch depth and refractive index of each of them are h and n_p respectively, the initial ($y=0$) widths of waveguide A and B are w_1 and w_2 . Let refractive indices and film thicknesses of another $p-1$ layers be n_1, n_2, \dots, n_{p-1} and t_1, t_2, \dots, t_{p-1} respectively. Due to asymmetry in the guided structure A, its width and propagation constant changes with length y ($y=0$ to L_c), while waveguide B has constant value of width and propagation constant throughout the length. Effective index method can be applied to calculate the value of propagation constant and effective

index of guided structure at each point ($y=0$ to L_c), in the fig.4.5 the equivalent structure is shown. Assuming that a field is launched in waveguide A, which after the coupling length will be transferred to waveguide B. The normal mode fields are evaluated for the tapered waveguide structure in a similar manner to that of the previous section and coupling length are found.

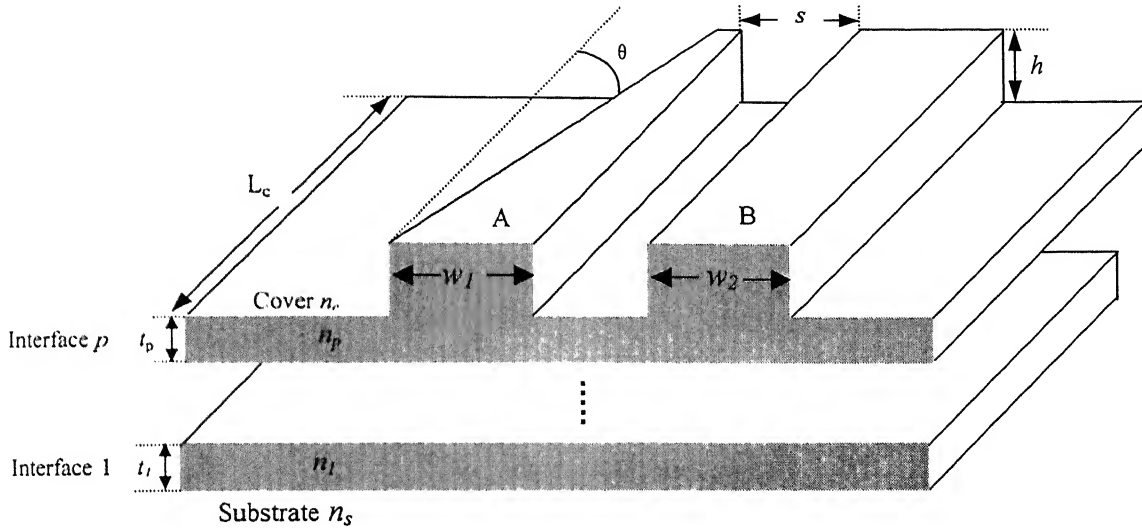


Figure 4.4 Schematic representation of multilayer asymmetrical coupler in which one waveguide is parallel while another is tapered.

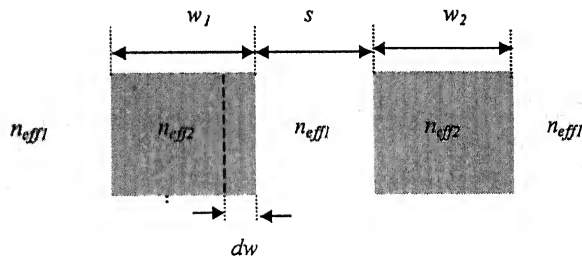


Figure 4.5 Equivalent waveguide representation of multilayer asymmetrical coupler

4.2.2 Double Tapered Coupler

A typical geometrical structure double tapered waveguide coupler is shown in fig 4.6. The structure is similar to single tapered coupler except both the rib waveguides A and B are tapered with tapering angle θ , the separation of waveguides is s , which will remain constant throughout the length. Again effective index (EI) and characteristic

matrix method, which is discussed earlier used to calculate coupling length of the waveguide, so the equivalent structure of the waveguide is converted into fig.4

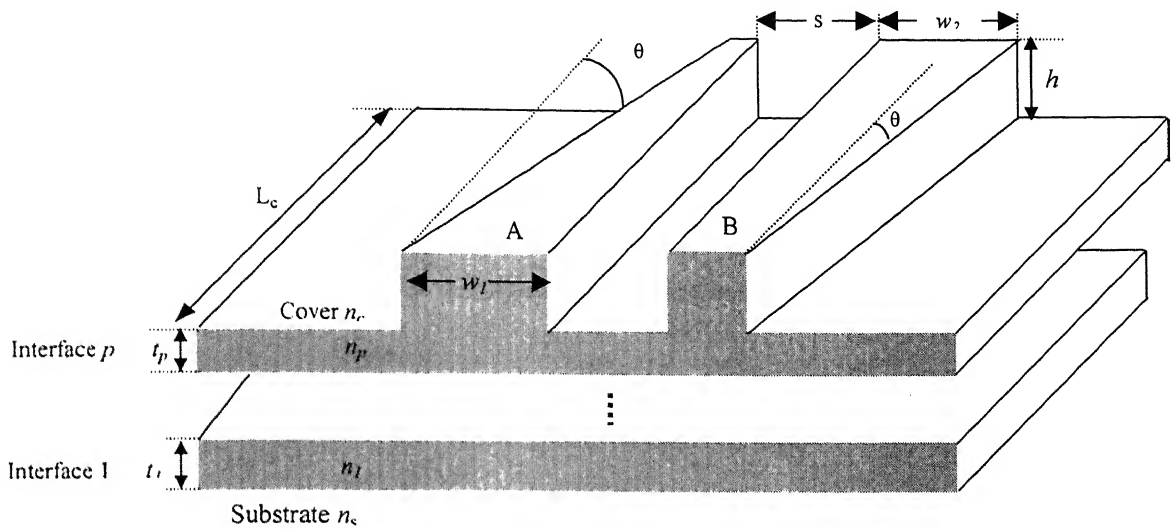


Figure 4.6 Schematic representation of multilayer asymmetrical coupler in which, both waveguides are tapered.

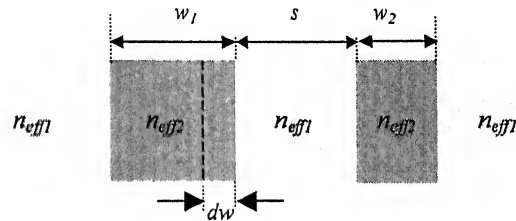


Figure 4.7 Equivalent waveguide representation of multilayer double tapered coupler.

RESULTS AND DISCUSSION

5.1 Slab Waveguide Characteristics

By the characteristic matrix method section.2.1, the complete dispersion relation in multilayer slab waveguides, the Eq. (2.33) and Eq. (2.46) represents for TE and TM guided modes respectively have been evaluated for a normalized propagation constant ' V '. For different guided structures the normalized wavelength dependent characteristics for TE and TM modes (b - V) curve are shown in fig.5.1, fig.5.2 and fig.5.3 for 4,5 and 6 layers respectively.

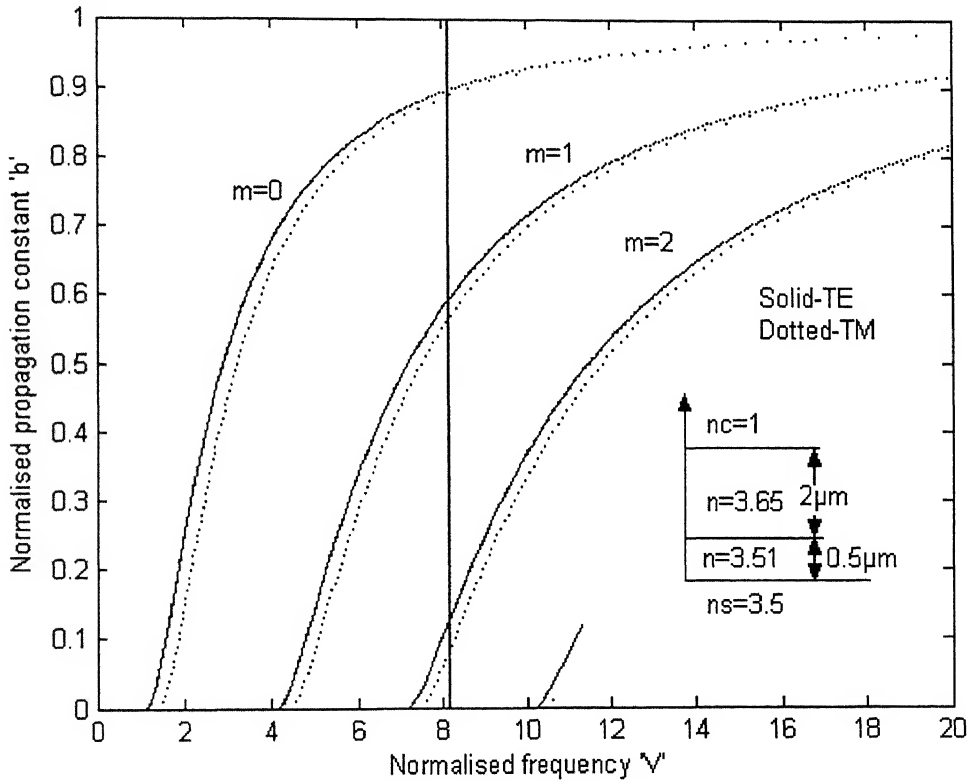


Figure 5.1 Plot of normalized propagation constant (b) against normalized frequency (V) for 4-layer slab waveguide.

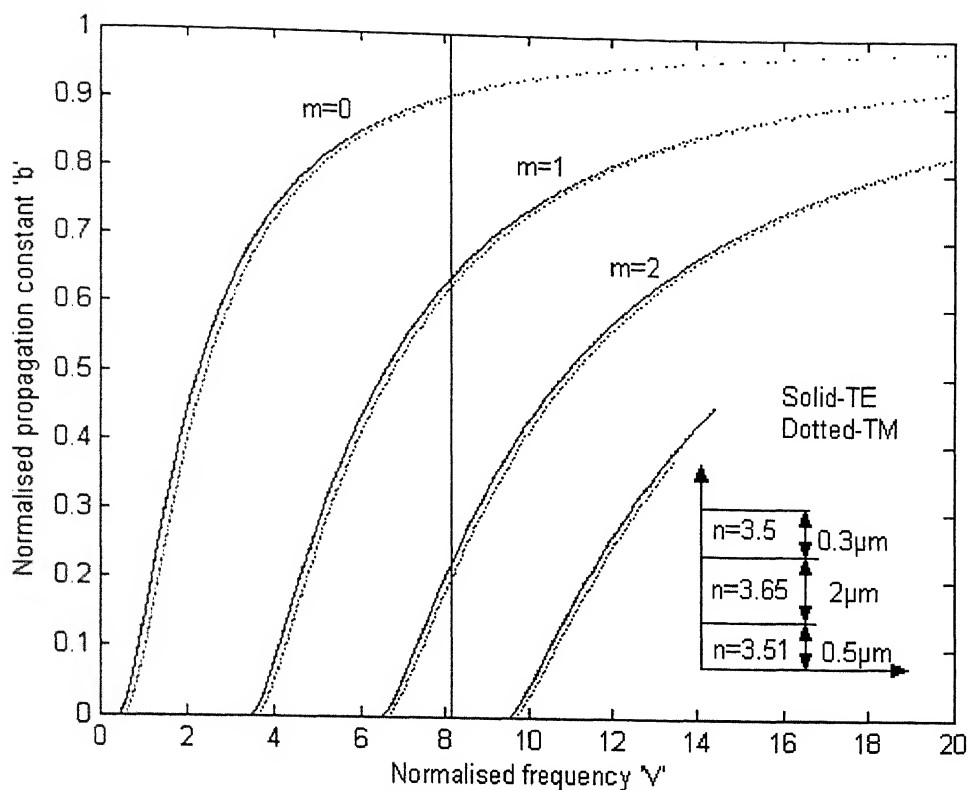


Figure 5.2 Plot of normalized propagation constant (b) against normalized frequency (V) for 5-layer slab waveguide.

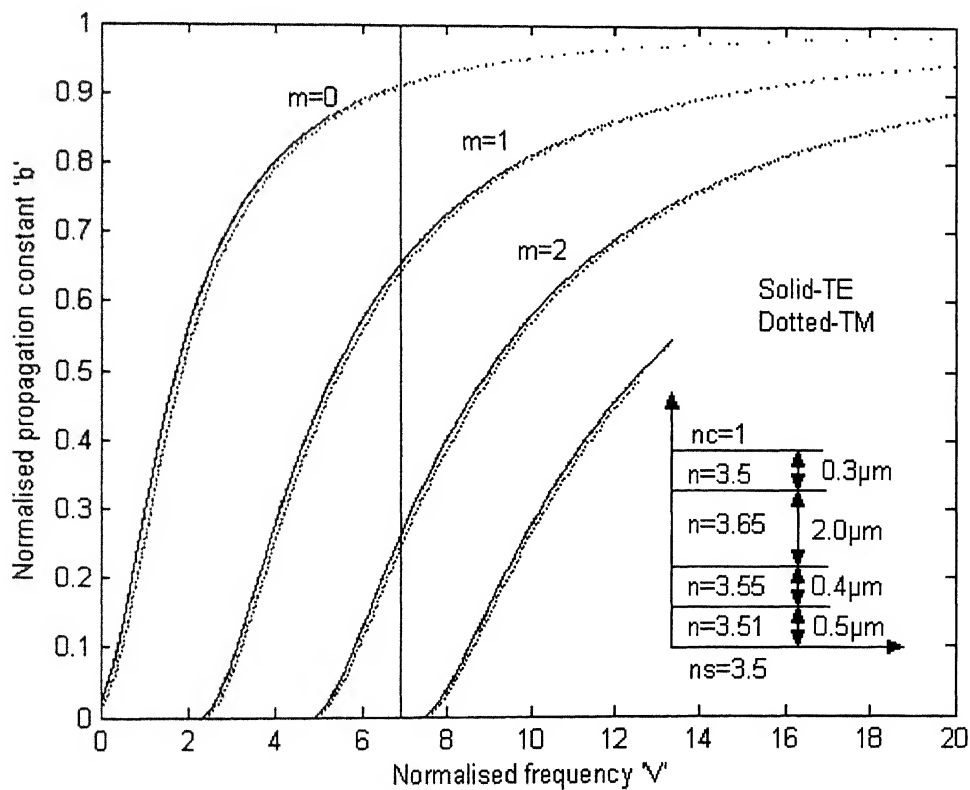


Figure 5.3 Plot of normalized propagation constant (b) against normalized frequency (V) for 6-layer slab waveguide.

5.2 Electric field (E) vs Distance (x)

The transverse electric (TE) and transverse magnetic (TM) field profile in the same 4,5 and 6 layers slab waveguide structure are shown in fig.5.4, fig.5.5 and fig.5.6 respectively. In all cases $n=3.65$ layer is assumed to be the guiding layer where the peak of the electric field lies. As expected, it is also observed that the evanescent tail is larger in the substrate than in the air.

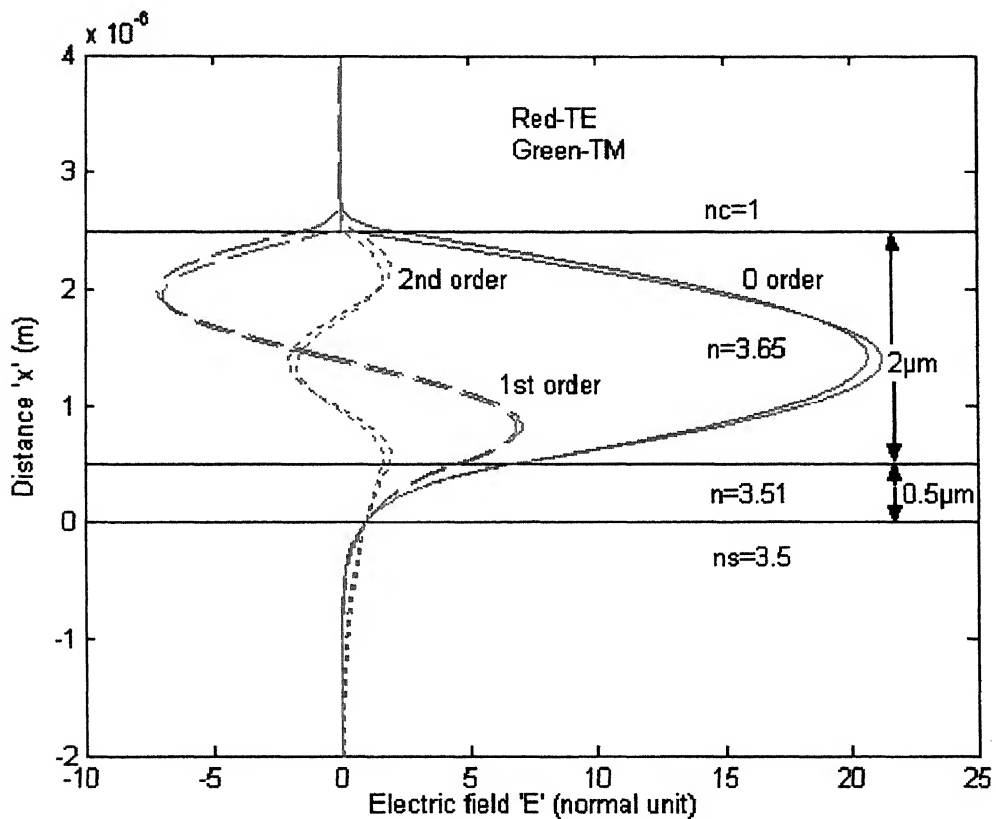


Figure 5.4 Plot of electric field (E) against distance (x) for 4-layers slab waveguide.

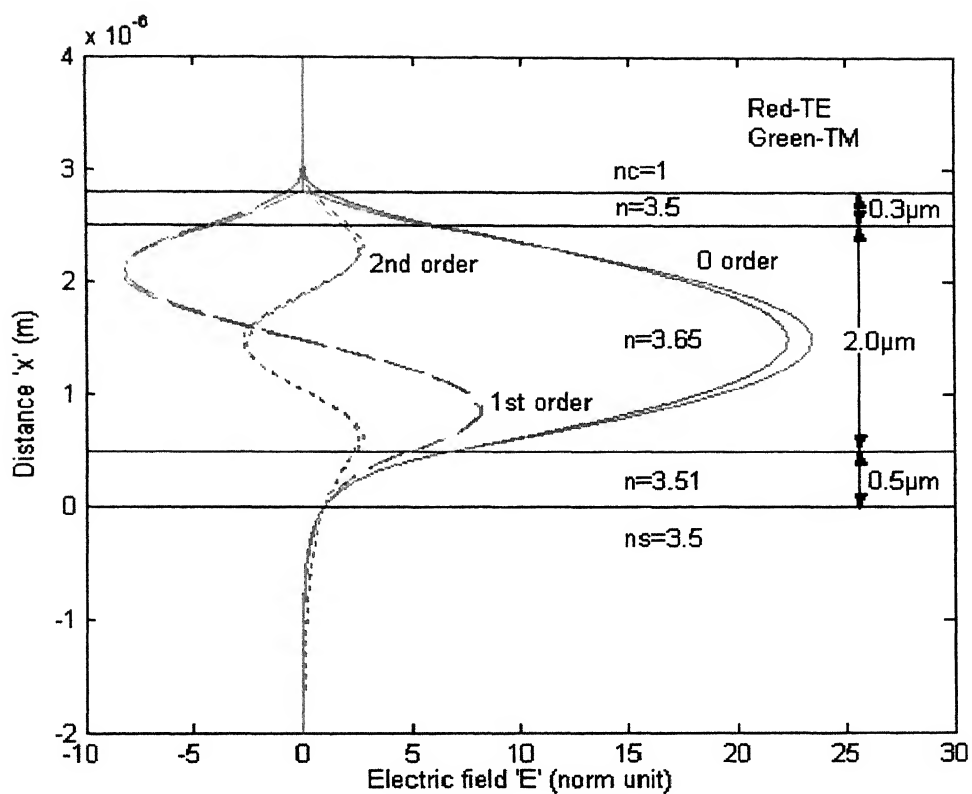


Figure 5.5 Plot of electric field (E) against distance (x) for 5-layers Slab waveguide

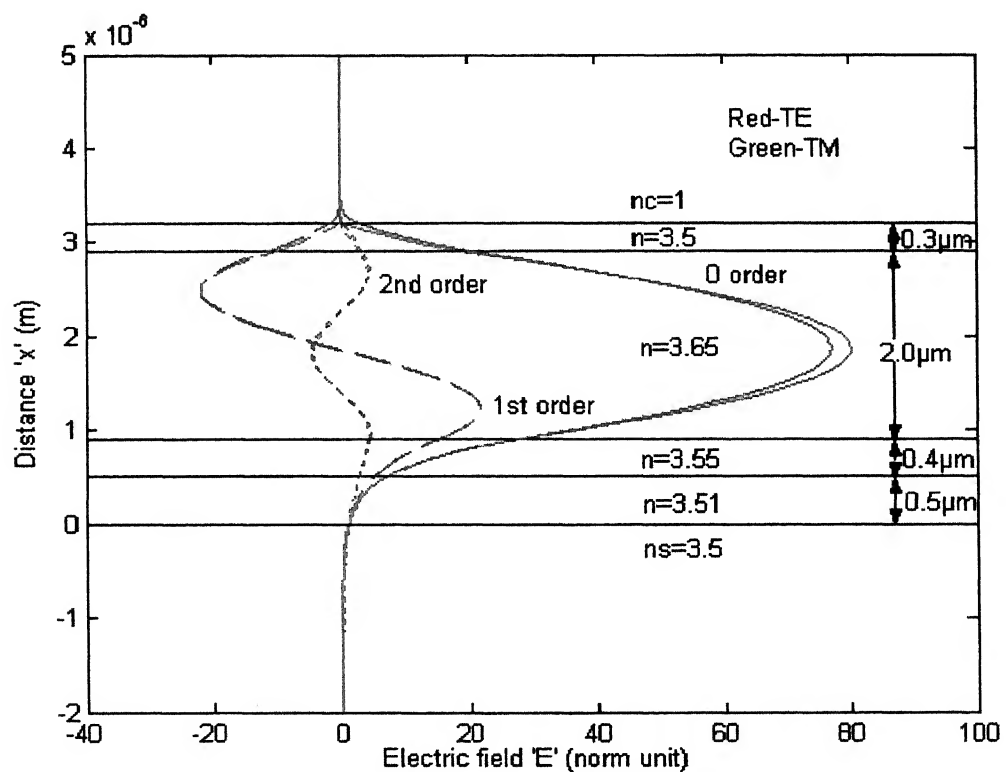


Figure 5.6 Plot of electrical field (E) against distance (x) for 6-layers slab waveguide

5.3 Single Mode Rib Waveguide Characteristic

The effective index method, which is discussed in section 3.1.1, we can calculate the effective index of central slice and lateral slice of rib structure now the whole structure is converted into three-layer slab waveguide, the effective indices of equivalent rib structure is shown in fig.3.2.

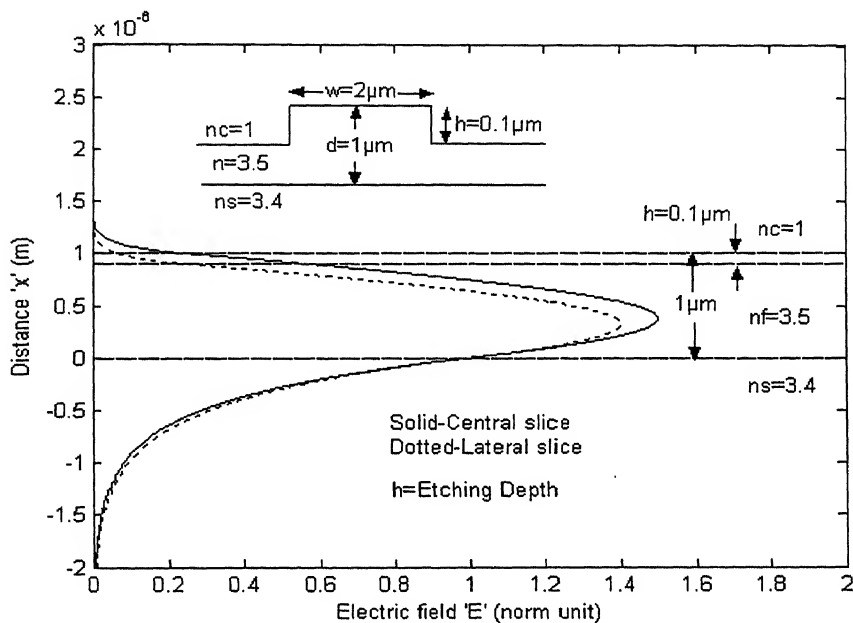


Figure 5.7 Electric field (E) profile in rib waveguide. Solid line represents profile in central slice where dotted profile line represents profile in lateral slice.

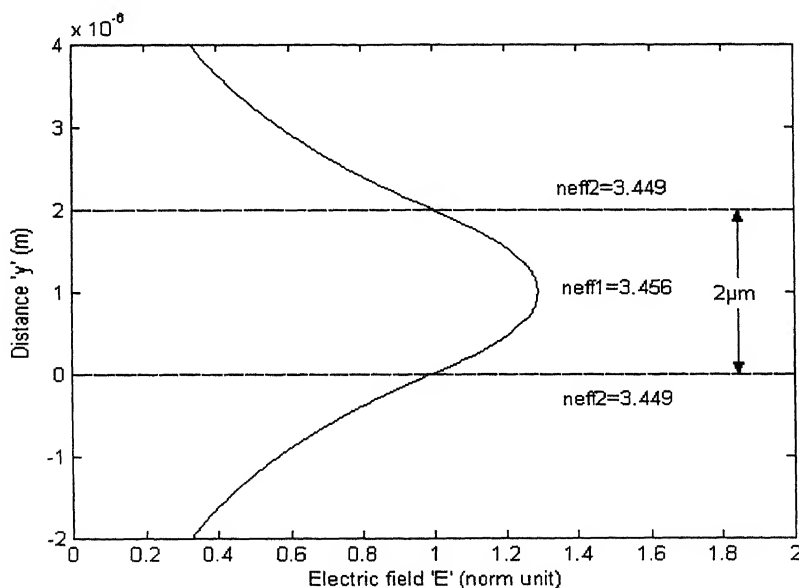


Figure 5.8 Electric field (E) distribution in the effective guided structure.

The fig.5.7 and fig.5.8, which is given above represents the electric field profile of the real structure and equivalent structure of rib waveguide respectively. Once we get the effective guided structure we draw the normalized propagation constant (b) vs normalized frequency (V) characteristic, as shown fig.5.9, by this curve we can calculate the effective index of equivalent rib structure.

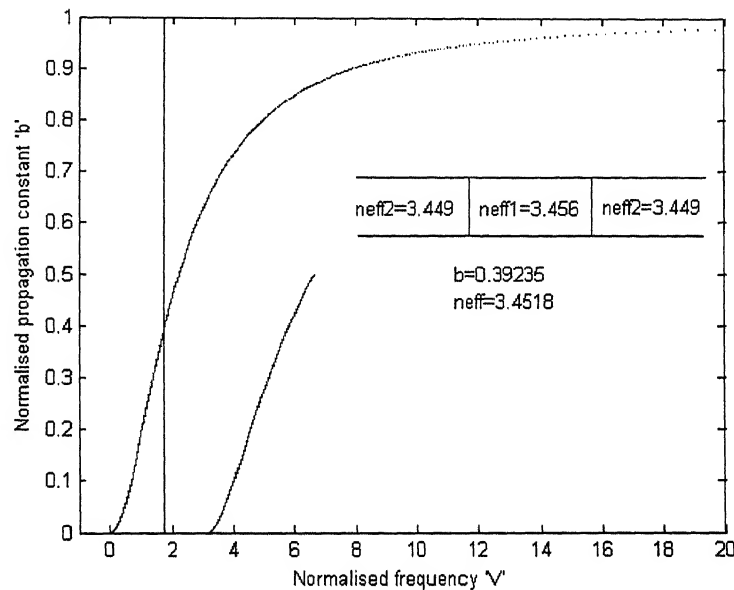


Figure 5.9 Plot of normalized frequency (V) against normalized propagation constant (b) for effective guided structure.

After calculating the effective indices of rib structure now we discuss the normalized propagation constant (b) vs width (w) of rib waveguide, fig 5.10 shows the profile for the given structure, by this figure it is clear that with increase of the value of width, normalized propagation constant increases. Another fig. 5.11 represents normalization propagation constant (b) vs wavelength (λ) characteristic, it is clear from this characteristic that with increase of the value of wavelength normalization propagation constant (b) decreases. Fig.5.12 shows the normalized propagation constant vs etching depth (h) characteristic for the given structure, from this figure it is clear that with increase of the value of etching depth, normalized propagation constant (b) increases, if

etching is keep on increasing a point come when lateral slice completely removed and characteristic become straight line.

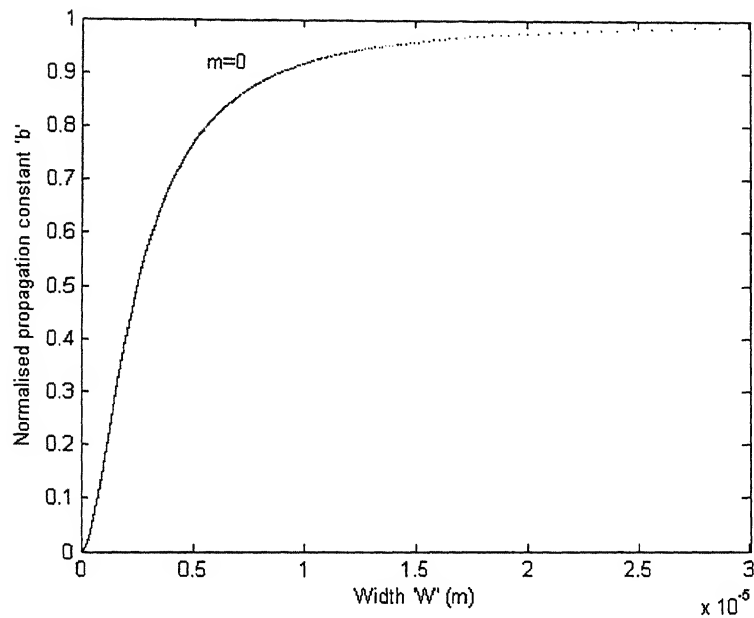


Figure 5.10 Plot of normalized propagation constant (b) against width (w) for single layered rib waveguide.

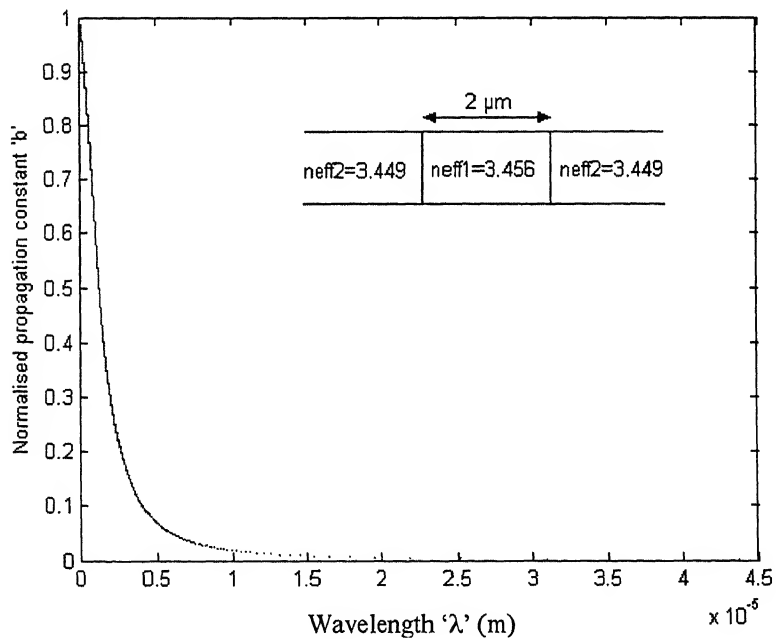


Figure 5.11 Plot of normalized propagation constant (b) against wavelength (λ) for effective guided structure

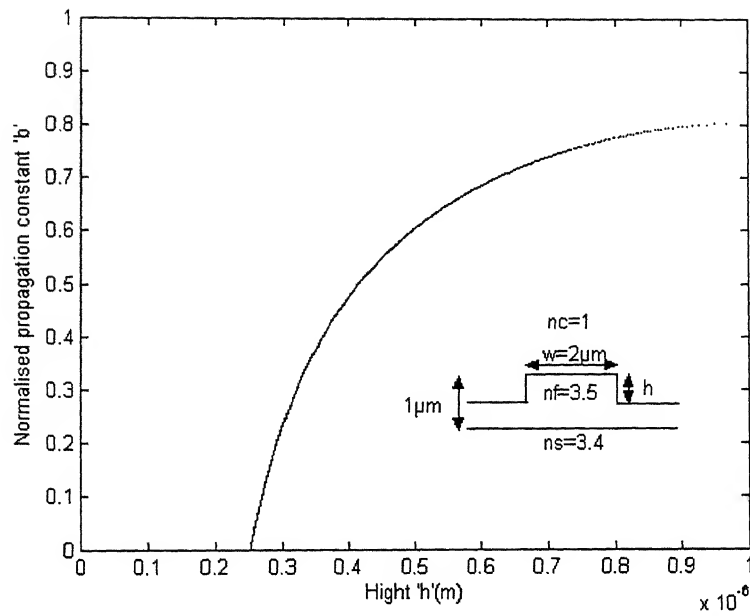


Figure 5.12 Plot of normalized propagation constant (b) against etch height (h) for single layered rib waveguide

The fig.5.13 shows the electric field profile in the rib structure, at $y=0$ signal is launched in the wave guide and it propagates throughout the length L ,

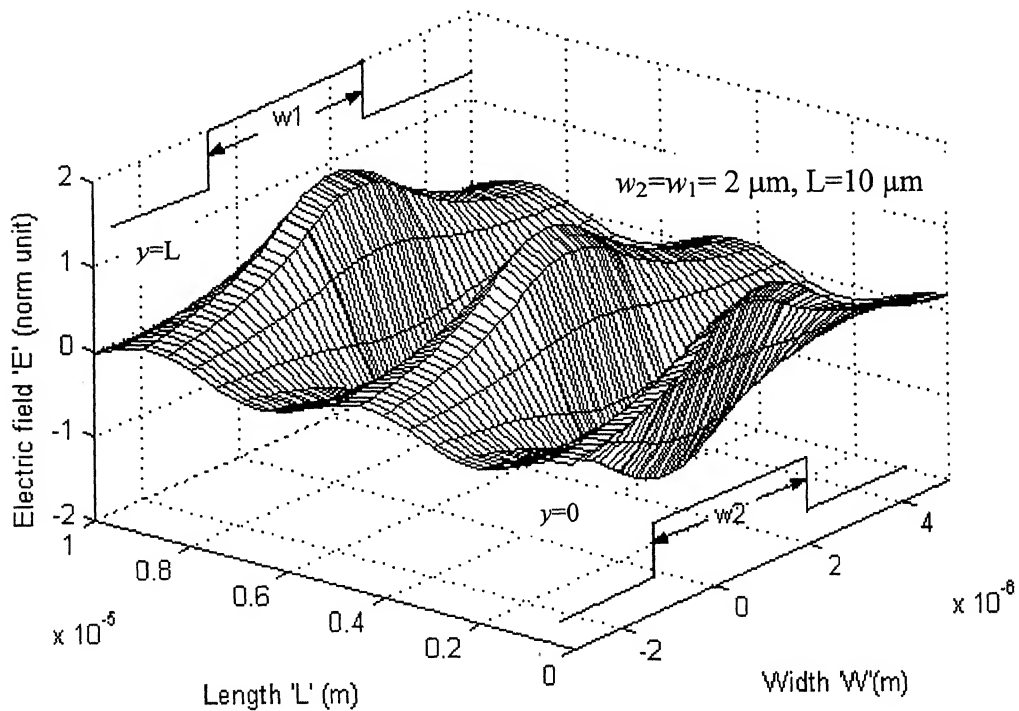


Figure 5.13 Electric field (E) distribution in single layered rib waveguide with respect to length (L) and width (w).

it is noted that field profile does not changes throughout the length it is because of, the propagation constant β does not change with change in length. In fig.5.14 power distribution characteristic of rib waveguide is shown, it is clear from this figure that power distribution throughout the whole structure will remain constant, it will not varied with change in distance.

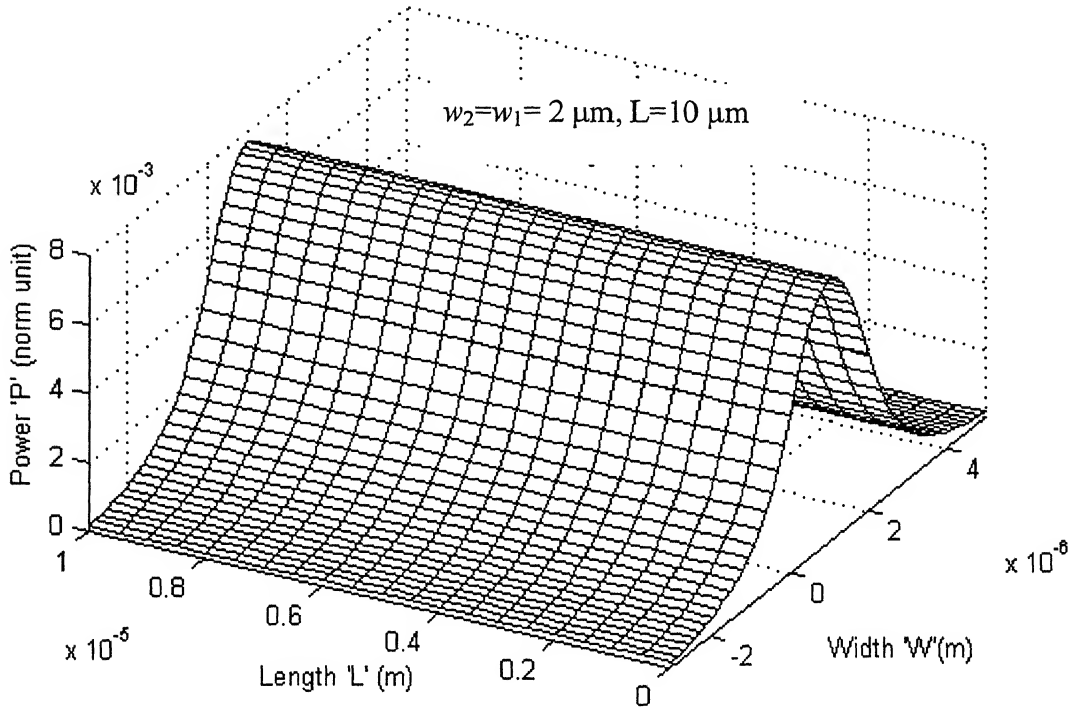


Figure 5.14 Distribution of power (P) in single layered rib waveguide with respect to length (L) and width (w).

5.4 Quantum Well Waveguide

The structure of quantum well is shown in section 3.2, by the help of Eq. (3.3) and Eq. (3.4) we can calculate the refractive index of the quantum well structure so the real structure converts into multilayer slab waveguide. The quantum well structure in the equivalent waveguide is work as a film and most of the signal propagates through this only. The figure, which is given below, shows the normalized propagation constant (b) vs normalized frequency (V) characteristic for equivalent quantum well waveguide, both the TE and TM propagating modes are represented by solid and dotted lines respectively.

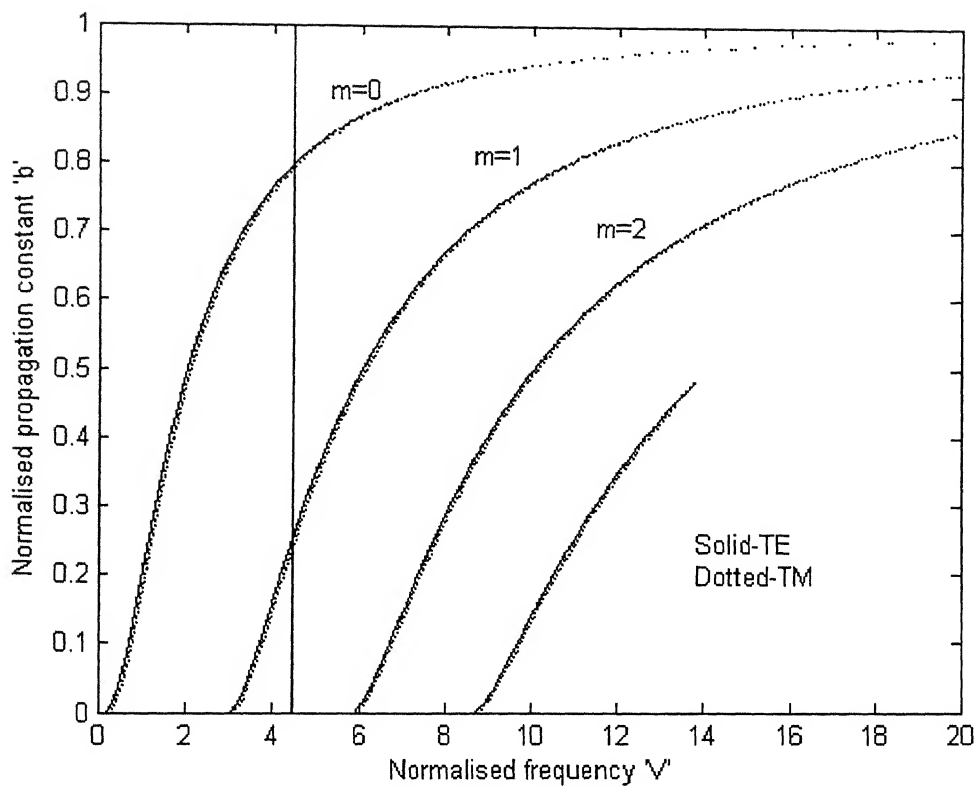


Figure 5.15 Plot of normalized propagation constant (b) against normalized frequency (V) for quantum well waveguide.

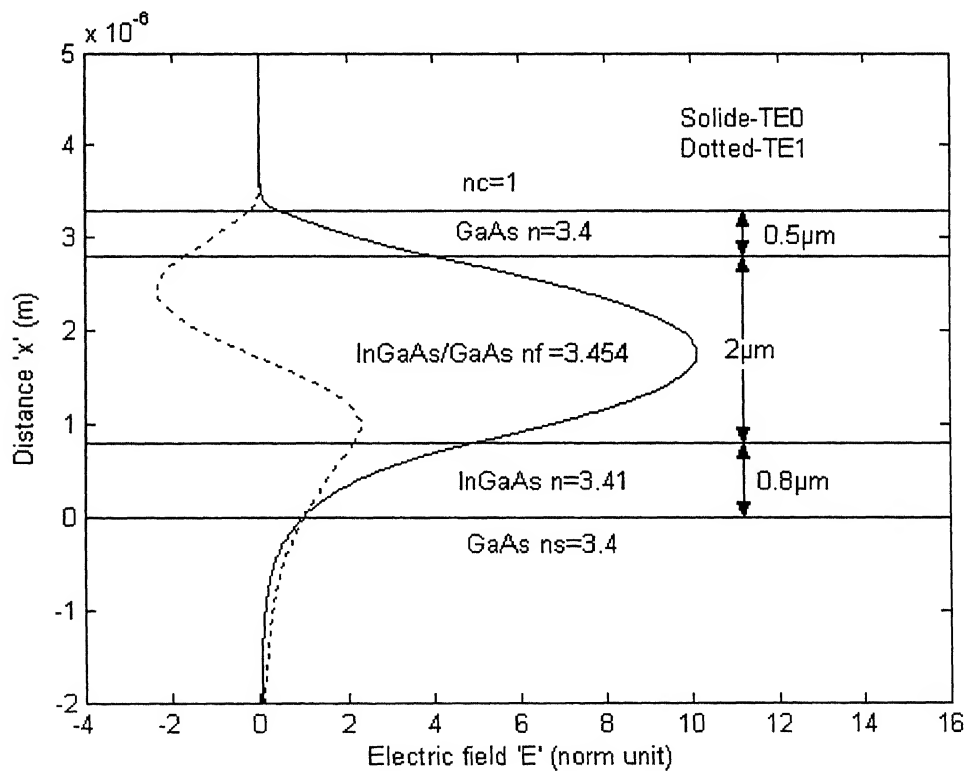


Figure 5.16 Electrical field (E) distribution in quantum well waveguide at different distances (x).

From the fig.5.15 it is clear that for TE and TM modes only two, zero order and first order mode will propagate in the given waveguide structure, the electric field in substrate, cladding and central layers can be calculated by Eq. (2.21), Eq. (2.31) and Eq. (2.26) respectively. The electric field profile for equivalent structure is shown in fig.5.16.

5.5 Tapered Waveguide

The structure of tapered waveguide is shown in section 3.3, it is simply a rib waveguide except it's width varies from one end to another end, due to variation in waveguide width the propagation constant of rib structure changes while etched section remain unchanged. For the calculation of propagation constant, the whole length of waveguide is divided into number of thin slices of thickness dy , where y varies from 0 to L .

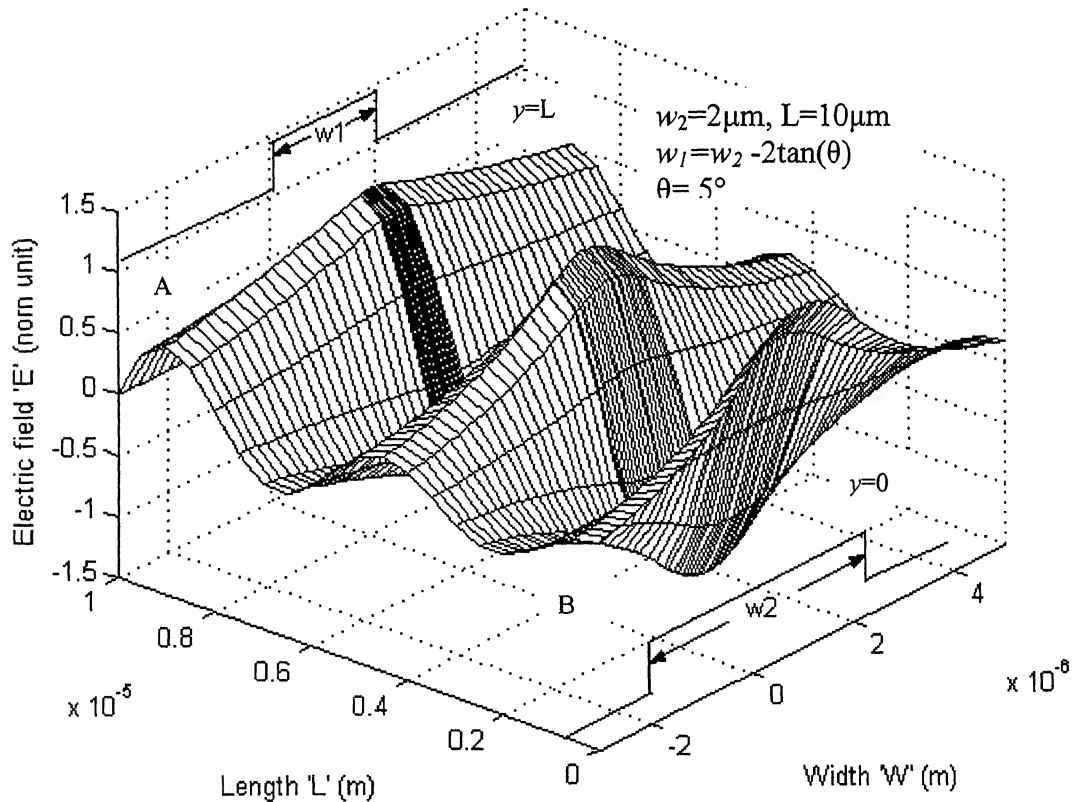


Figure 5.17 Electric field (E) distribution in taper waveguide with respect to length (L) and width (w).

Now by the effective index method, effective indices and propagation constants for each slice can be calculated, finally it is clear that the effective index and propagation constant increases with decreases in waveguide width. The affect of this increase in propagation constant and effective index is that the signal weakly guided at smaller width side with respect to larger width side, fig.5.17 shows the electric field profile for given waveguide structure, at the end A signal is launched to the waveguide when it propagates, the value of propagation constant (β) increases, at the end B propagation constant attains maximum value while A attains the minimum value.

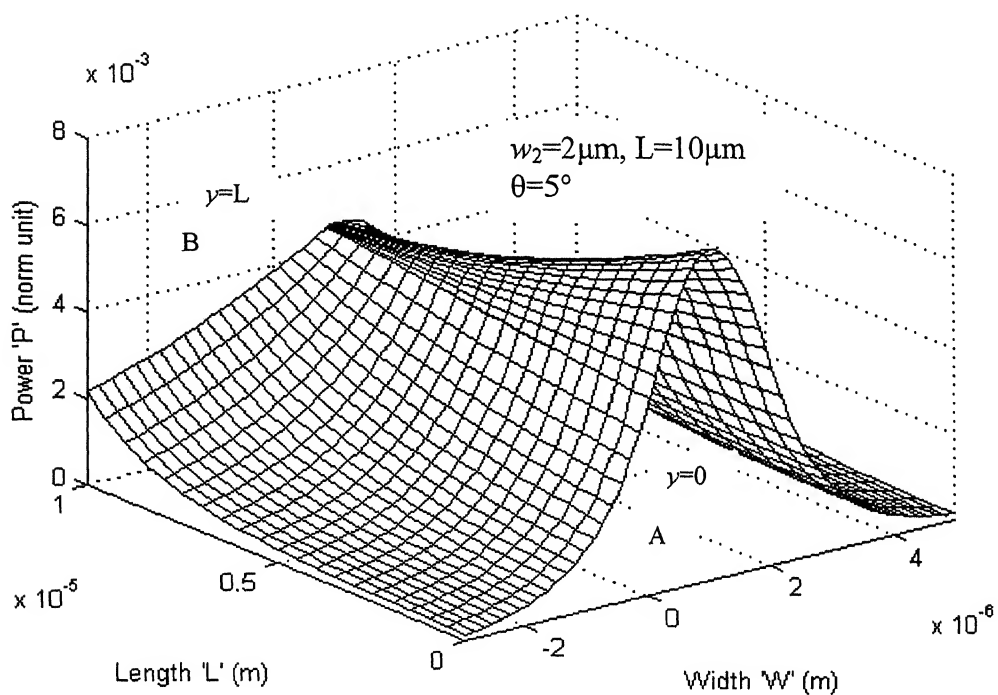


Figure 5.18 Distribution of power (P) in taper waveguide with respect to length (L) and width (w).

The above fig.5.18, shows the power distribution characteristic for tapered waveguide, with increase in propagation constant with distance (y) its profile changes at end B amplitude of power is very much reduces from the previous value, it means most of the power lost out of the rib structure.

5.6 Couplers

5.6.1 Parallel Coupler

In the section 4.1.1 we have discussed the structure of parallel coupler, it is simply two parallel waveguides of different width w_1 and w_2 , which is separated by a distance ' s ', the geometrical structure is shown in fig.4.2,

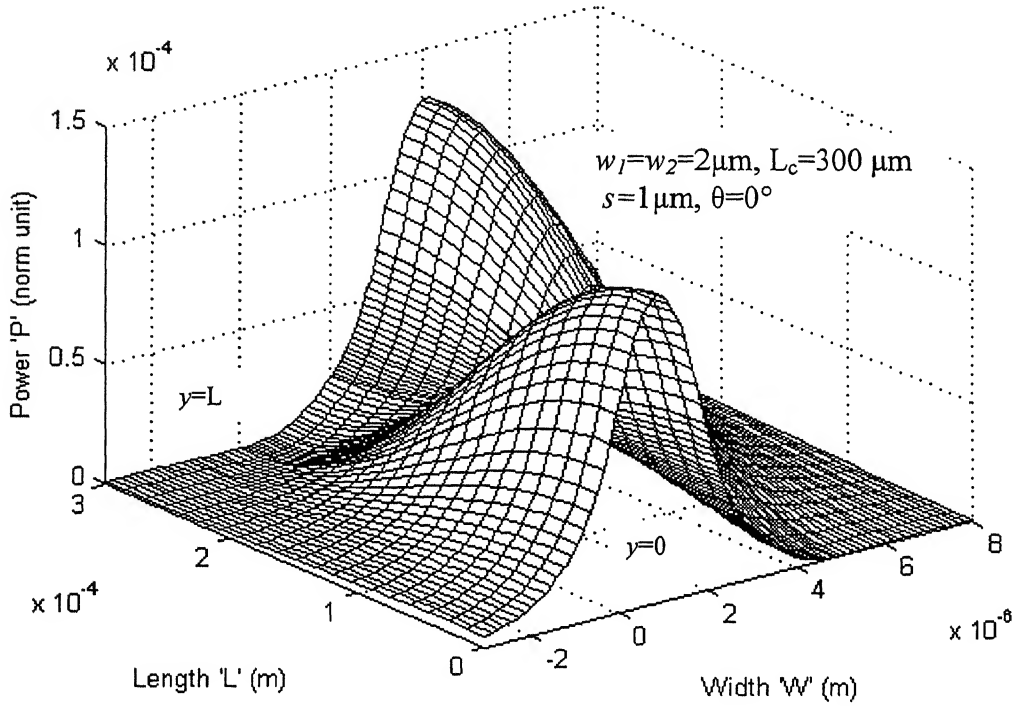


Figure 5.19 Distribution of power (P) in symmetrical parallel optical coupler.

apply the effective index method to calculate the effective indices of the actual waveguide structure, now the real waveguide structure converts into 5-layers waveguide, which is shown in fig.4.3. The fig.5.19 represents the power distribution characteristic of parallel coupler, at the end $y=0$ energy is launched to the waveguide A and it will completely coupled to the waveguide B after certain length L_c , this length is known as coupling length (L_c). The simulation result shown in fig.5.19, it is clear that coupling length L_c for given parallel coupler is $300\mu\text{m}$, which is near to $260\mu\text{m}$ calculated by Eq. (4.24).

5.6.2 Tapered Coupler

5.6.2.1 Single Tapered Coupler

Tapered coupler is similar to parallel coupler except its one waveguide is tapered in shape, by effective index method the effective indices of actual waveguide can calculate. In the earlier section 5.5 we have discussed the method how to calculate the effective index of tapered waveguide, similar method we will apply here to calculate the effective index of tapered waveguide.

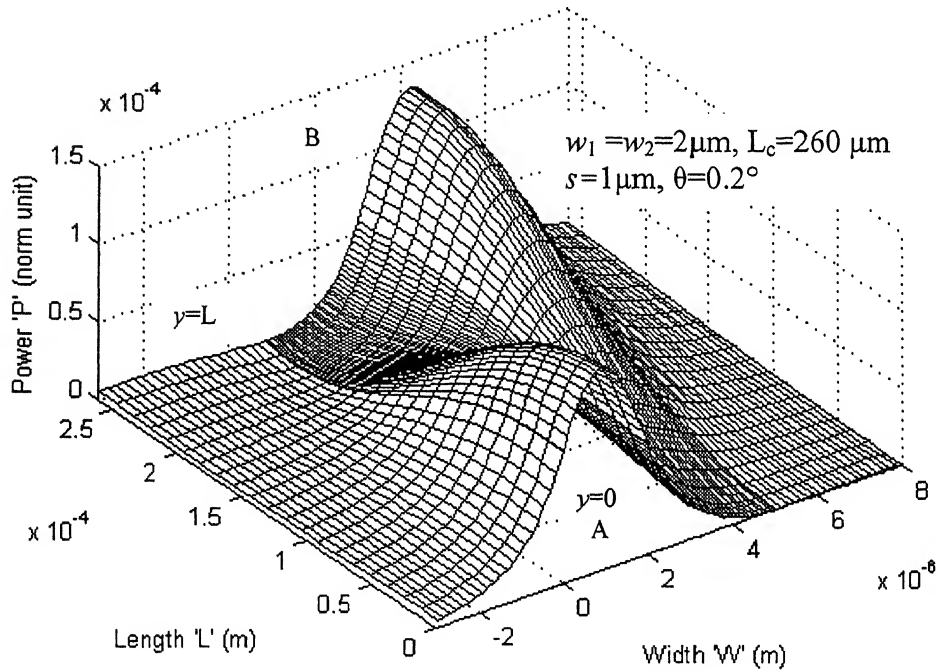


Figure 5.20 Distribution of power (P) in single tapered optical coupler.

Now the actual waveguide structure is converted into 5-layer waveguide, shown in fig. 4.4, which can be easily solved by characteristic matrix method given in section 2.1. The simulation result, which is shown in above fig. 5.20 it is clear that coupling length L_c for given tapered coupler ($\theta = 0.2^\circ$) is $260\mu\text{m}$, which is much less than $300\mu\text{m}$ for parallel coupler, the plot of coupling length (L_c) against tapering angle (θ) as shown in fig. 5.21, it is clear that effective index of tapered waveguide changes with change in length.

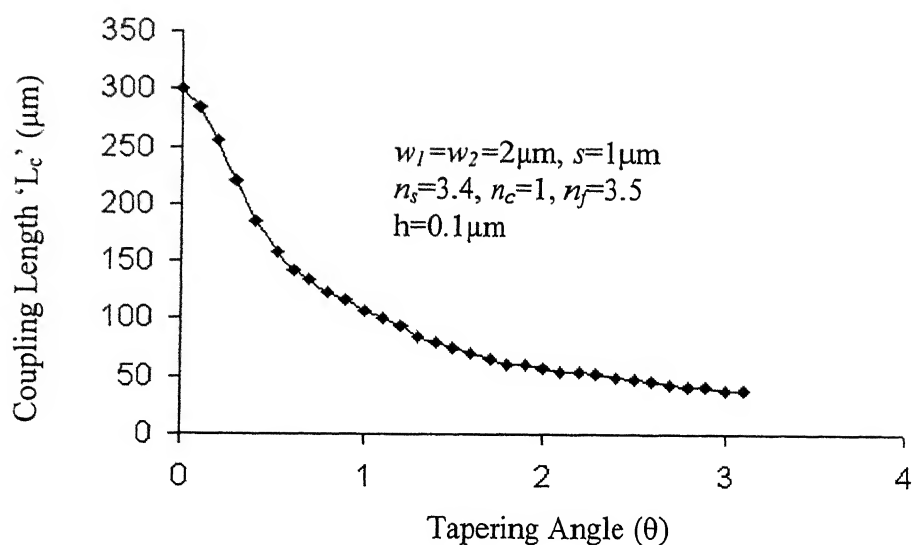


Figure 5.21 Variation of coupling length (L_c) with tapering angle (θ) for single tapered coupler

5.6.2.2 Double Tapered Coupler

In the double tapered coupler, both waveguides are tapered at one end and separated by a constant distance ' s ',

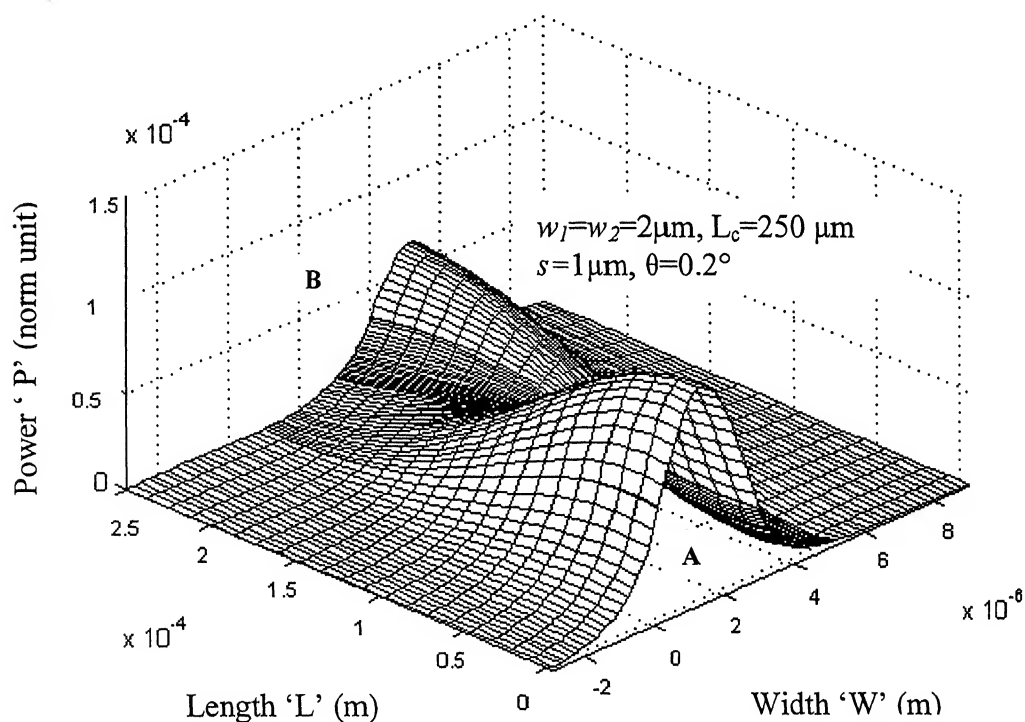


Figure 5.22 Distribution of Power (P) in double tapered coupler

if any signal is launch in waveguide A then it will coupled in waveguide B after coupling length (L_c), the fig. 5.22 represents the power distribution curve in double tapered coupler, the coupling length (L_c) vs tapering angle (θ) characteristic of double tapered coupler for different separation (s) of waveguides is shown in fig. 5.23.

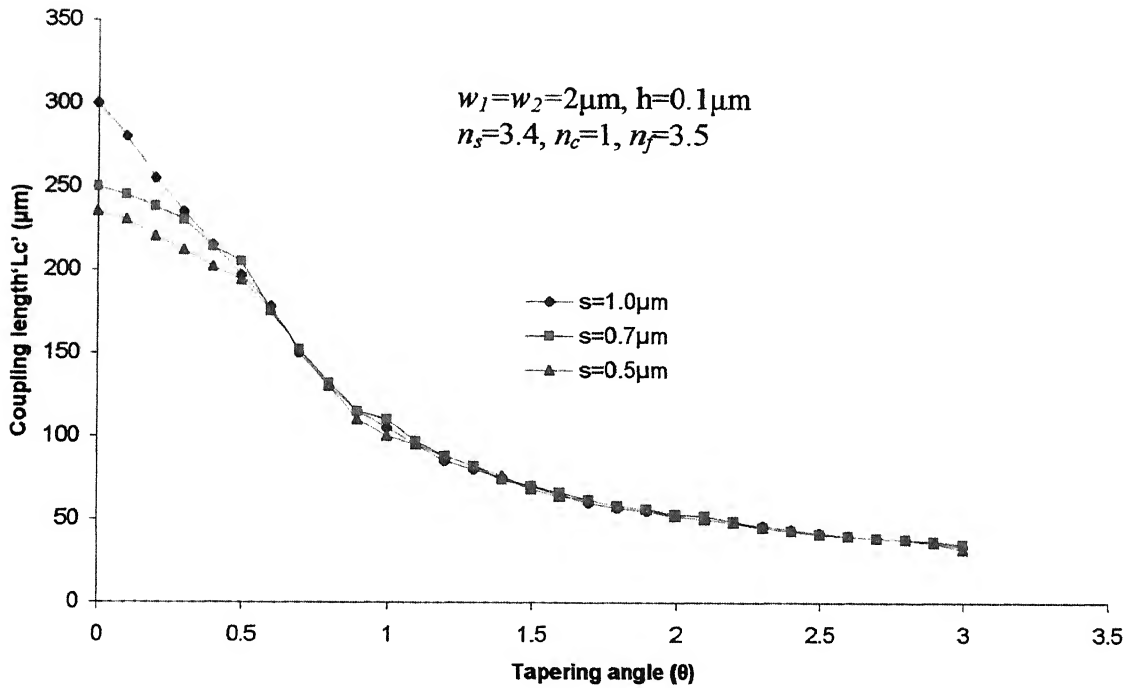


Figure 5.23 Variation of coupling length (L_c) with tapering angle (θ) for double tapered coupler.

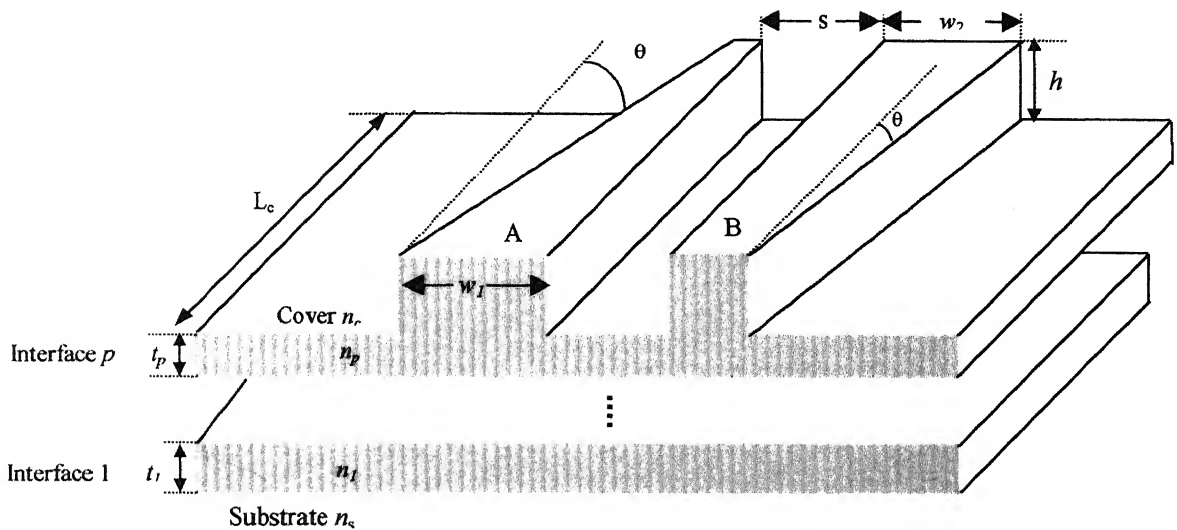


Figure 5.24 Schematic representation of multilayer asymmetrical coupler in which, both waveguides are tapered.

The insertion Loss in directional coupler $= 10 \log \frac{P_i}{P_o}$ dB

Where P_i = Input power launched in waveguide A at $y=0$

P_o = Output power from waveguide B at $y=L_c$

Couplers	w_1 (μm)	w_2 (μm)	S (μm)	θ/θ ($^\circ$)	Coupling Length L_c (μm)	Insertion Loss (dB)
Symmetrical Coupler	2.0	2.0	0.5	0/0	300	0.1873
			0.7	0/0	250	0.1643
			1.0	0/0	232	0.1434
Single Tapered Coupler	2.0	2.0	1.0	0.2/0	260	0.9404
Double Tapered Coupler	2.0	2.0	0.5	0.2/0.2	234	2.2495
			0.7	0.2/0.2	238	3.7444
			1.0	0.2/0.2	255	6.4588
			0.5	1.0/1.0	100	5.2149
			0.7	1.0/1.0	105	5.2155
			1.0	1.0/1.0	110	6.2215
			0.5	1.5/1.5	68	5.5695
			0.7	1.5/1.5	70	8.0612
			1.0	1.5/1.5	70	9.7828

Chapter 6

Conclusion

Three-layer semi-infinite dielectric waveguide have been studied earlier, but this method is not suitable for N-period stack or multilayer waveguide so special methods has been developed for the determination of guided mode and dispersion equation, the numerical technique, characteristic matrix method, is introduced here for the determination of guided modes in multilayer optical waveguide, in this method transverse electric (TE) and transverse magnetic (TM) where deal separately. This characteristic matrix method is a generalized method, which is applicable for any kind of waveguide structure; by the strict investigation into dispersion relations for multilayer systems we can plot the normalization propagation constant (b) against the normalized frequency (V) characteristic, by this characteristic we can calculate the effective index and the number of propagated modes in the waveguide structure, once we get the effective index of guided structure we can plot the electric and magnetic field distribution in the waveguide structure. The application of this method has been carried out for the mode field and intensity distribution of planar waveguides. Coupling between optical waveguides can be treated as a five-layer medium problem. Such a five-layer medium consists of two guiding layered with higher index of refraction, spaced by a central layer with lower index of refraction. A MATLAB program has been developed to implement the characteristic matrix method. The simulation result represents the power distribution characteristic in symmetrical, and asymmetrical (Single and Double tapered coupler). Finally it is concluded that coupling length reduces with increase in tapering angle (θ) for both single and double tapered coupler and for same tapering angle (θ) the coupling length reduces with decrease in separation (s) of two waveguides.

REFERENCES

- [1] H. Kogelnik and V. Ramaswam, "Scaling Rule for Thin-Film Optics Waveguide", Appl optics., Vol.13, No.8, August 1974.
- [2] Henri P.Uranus and M.O. Tjia, " Determination of Mode Field profile and Its Evolution in Planar waveguide with Arbitrary Refractive Index Profile using Characteristic Matrix Method", Proc.of the International Conf. On Electrical, Electronics, Communications, and Information (CECI 2001) Jakarta-Indonesia, March 7th-8th, 2001.
- [3] Pallabh Bhattacharya, "Semiconductor optical Devices", Prentice Hall of India Private Limited, 1999.
- [4] Utpal Das and Pallabh K. Bhattacharya, " Variation of reflective index strained $\text{In}_x\text{Ga}_{1-x}\text{As}$ -GaAs hetrostructures", J Appl. Phys., Vol.58, No. 1, 1 July 1985.
- [5] Ajoy Ghatak and K. Thyagaragan, " Optical Electronics", Cambridge University press, 1991.
- [6] Keigo iizuka, "Elements of photonics Volume 2 for fiber and integrated optics", A John Wiley & Sons, INC., Publication 2002.
- [7] Tamir T, "Integrated Optics", Springer-Verlarg, New York, 1975.
- [8] A.Yariv, P.Yeh, "Optical Waves in Crystals", John Wiley & Sons publication 1984.
- [9] A.Yariv, "Coupled-mode theory for guided wave optics," IEEE J.Quantum Electron., Vol. QE-9, pp.919-933, Sept.1973.
- [10] R.Thommas Hawkins II and Jeffrey H.Goll, "Method for calculating coupling length of Ti:LiNbO_3 waveguide directional coupler", Journal of Lightwave Technology., Vol.6, No.6, June 1988.

- [11] John Chilwell and Ian Hodgkinson, "Thin-films Field transfer Matrix Theory of Planar Multilayer Waveguides and Reflection from Prism-loaded Waveguides", J. Opt. Soc. Am. A., Vol. 1, No. 7, pp. 742-753, July 1984.
- [12] W.Streifer.D.R.Scifres, and R.D.Burnham,"Coupling coefficients for distributed feedback single-and double-heterostructure lasers", IEEE J.Quantum Electron., Vol. QE-11, pp.867-873, 1975.
- [13] Emmanuel Anemogiannis, Elias N. Glytsis and Thomas K. Gaylord, "Determination of Guided and Leaky Modes in Lossless and Lossy Planar Multilayer Optical Waveguides Reflection Pole Method and Wave vector Density Method", Journal of light wave technology., Vol 17, No.5, May 1999.